# ROLE OF TEMPERATURE AND SURFACE FINISH IN PREDICTING TOOL WEAR USING NEURAL NETWORK AND DESIGN OF EXPERIMENTS

By

**GAURAV BARTARYA**



**DEPARTMENT OF MECHANICAL ENGINEERING**

**Indian Institute of Technology Kanpur**

**FEBRUARY, 2002**

# ROLE OF TEMPERATURE AND SURFACE FINISH IN PREDICTING TOOL WEAR USING NEURAL NETWORK AND DESIGN OF EXPERIMENTS

*A Thesis Submitted*
*in Partial Fulfillment of the Requirements*
*for the Degree of*

**MASTER OF TECHNOLOGY**

*By*

**GAURAV BARTARYA**

*to the*

**Department of Mechanical Engineering**

**Indian Institute of Technology Kanpur**

**February, 2002**

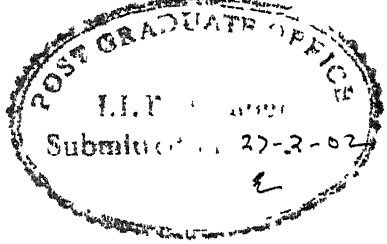


## Certificate

It is certified that the work contained in the thesis entitled **"Role of temperature and Surface finish in predicting tool wear using Neural Network and Design of Experiment"**, by **Gaurav Bartarya, Roll No.-Y010521**, has been carried out under my supervision and that this work has not been submitted elsewhere for any degree

**Dr. S.K.Choudhury**
Professor,
Deptt of Mechanical Engineering,
Indian institute of technology,
Kanpur,
India
Feb,2002

## Acknowledgement

I take this opportunity to express the feeling of sincere gratitude towards my thesis supervisor **Dr.S.K.Choudhury** for his expert guidance and encouragement, which have been the vital factors in successful completion of the present work

I would like to thank Mr H P Sharma of the Manufacturing Sc lab and Mrs Anjali Kulkarni of Robotics lab for their guidance and help in all the technical matters without which this work could not have been brought into reality A word of thanks also gose to Mr Phoolchand of Manufacturing Sc lab and Mr Rajendra of Robotics lab for their assistance during fabrication and the actual experimental work

It is indeed my great pleasure to express my sincere thanks to Mr Rakesh Mote, Mr Anil Rai and all my friends for their timely help and friendly co-operation in sorting out my problems and making my stay at IIT Kanpur pleasant and memorable one I am very much grateful to my parents who always supported me despite many problems in all the circumstances

**Gaurav Bartarya**

# Content

**List of figures** **Page number**

## List of Tables — Page number

# Nomenclature

V, F, D input parameters (cutting speed, feed and depth of cut)

v, f, d levels of above input parameters

x input variable

y response variable

$\beta_0$, $\beta_1$ unknown constants

$\varepsilon$ random error with mean zero and the variance

L least square function

n number of data points

$S_{xx}$ corrected sum of squares of x

$S_{xy}$ corrected sum of cross products of x and y

$b_i$ $i^{th}$ regression coefficient

$\Delta w_{ij}(n)$ change in the weight of connection between the $j^{th}$ neuron and the $i^{th}$ neuron in the previous layer for $n^{th}$ iteration

E(n) sum of squared errors over the output neurons

N total number of patterns in the training set

Ra Centerline average of the sur5face roughness

a, b constants of hyperbolic tangent function

$d_j$ desired response in the $j^{th}$ output neuron

$e_j$ error at the $j^{th}$ neuron

$n_1$ refractive index of the core material of the optical fiber

$n_2$ refractive index of the cladding material of the optical fiber

r number of neurons in the output layers

$v_j$ the net internal activity of the $j^{th}$ neuron

$w_{ij}(n)$ weight of the connection between the $j^{th}$ neuron and the $I^{th}$ neuron in the previous layer for the $n^{th}$ iteration

$x_i$ $i^{th}$ component of the input pattern

$y_j$ actual response of the $j^{th}$ neuron

$z_i$ $i^{th}$ component of the output pattern

$\alpha$ momentum constant

$\eta$ . learning rate constant

$\delta_j$ . local gradient at $j^{th}$ neuron

$\phi(x)$ : the activation function

$\theta_c$ · angle of incidence on the optical fiber

## Abstract

Tool wear is the most undesirable characteristic of the machining operation Tool life and surface quality of the work-piece are largely affected by the tool wear Flank wear is the predominant phenomenon, which leads to the tool failure Conventional tool change strategies are largely based on the operator's judgment or the most conservative estimate of the tool life This results into frequent tool change, under utilization of the cutting tool and the higher costs A reliable and sensitive technique to monitor the tool wear without interrupting the machining operation is most important for the fulfillment of the modern machining concepts like unmanned machining or the Factories of future (FOF) There are many techniques suggested by different researchers to predict the tool wear The present work focuses on the two of those techniques, namely "Design of Experiments" and the "Neural Network" In the present work, the response (output) variables, measured during turning of the EN-24 steel with tool of HSS with 10% cobalt, are flank wear, surface finish and cutting zone temperature Input parameters are the cutting speed (in m/min ), feed (in mm/rev ) and the depth of cut (in mm) The predictions for all the three response variables are obtained with the help of empirical relation between different responses and input variables using Design of Experiments (DOE) and also through Neural Network (NN) program The predicted values of the responses, by both the techniques i e DOE and NN are compared with experimental values and their closeness with the experimental values is found out Relationship between surface roughness and the flank wear and also between the temperature and the flank wear are found out for indirect measurement of the flank wear with the help of surface roughness and cutting zone temperature

# *Chapter 1*

## Introduction

In today's world of manufacturing, which is heading towards more and more automation, the unattended machining is the latest concept But the very limitation of the unattended machining is the wear and breakage of the tool It is very important to measure the tool wear on line so that the tool can be changed when its profile is lost or it is producing bad quality product So the measurement of the tool wear on-line is the most sought after thing in unattended manufacturing

The problem of on-line tool wear measurement in machining operations has got active attention from the researchers and a lot of work is done in this field This is because tool change strategies, product quality, tooling cost and productivity, are all influenced by tool wear

Tool wear can be predicted by sensing various parameters like cutting force, temperature, torque, vibrations, surface roughness, acoustic emission, current, power etc as all these parameters relate with tool wear

## 1.1 Tool wear in metal cutting

Usually tool fails because of

- Plastic deformation due to high forces and temperature
- Mechanical breakage due to the weakening of the tool
- Gradual wearing due to the rubbing of the rake face by the chip and flank face by the machined surface

### 1.1.1 Types of tool wear

Progressive tool wear is of two types

1- **Flank wear:** It takes place on the flank face and primary cutting edge due to the rubbing between flank face and the machined surface

2- **Crater wear:** On the rake face, due to the friction between chip and the rake face

Crater wear is due to the diffusion process between tool and the chip, which is a phenomenon occurring at higher speeds and higher temperature By controlling the speed of machining the crater wear can be minimized Flank wear is more dangerous as it can change the work-piece's specifications, and therefore, it needs more attention

Tool wear leads to

1- Increase in cutting force and subsequently increase in power consumed in metal cutting
2- Increase in dimensional instability of the work-piece
3- Change in cutting conditions
4- Deterioration of the surface finish of the job produced
5- Increase in machine vibrations

A cutting tool is said to be worn out if it is unable to produce work-piece of required dimensions and surface finish

### 1.1.2 Mechanism of tool wear

Tool wear occurs due to rubbing between tool and work-piece or tool and chip (due to the friction between them) This wear may be due to one or more following causes,

viz adhesion, abrasion, diffusion, fatigue, progressive wear under sliding conditions and plastic deformation

1-Adhesion

When the two surfaces come in close contact, strong bonds are formed due to welding of surface asperities If bond formed on the asperity junctions are stronger than local strength of material, particle may transfer from one junction to the other (means, from tool to chip), when junction fails

2-Abrasion

When the two surfaces are in sliding contact, the surface asperities of the harder material plough a series of grooves on the softer material Material removal may also be due to hard particles trapped at the sliding surface Thus the abrasive wear to take place, one the material of pair of sliding surface must be harder than the other

Both the adhesion and abrasion are predominant at low and moderate cutting speeds

3-Diffusion

It's a process of atomic transfer at contacting asperities, depending upon relative affinity of atoms This cause wear by leading to change in physical properties such as hardness, toughness etc. of either the tool material or work material, or both The diffusion process occurs at the chip tool interface, where the high temperature and pressure exists

4-Fatigue

When one material is sliding over other, each asperity of the material associated with a wave of deformation At some distance ahead of the asperity, the underlying material is compressed, and behind the asperity, tensile stresses elongate the material This

alternating stress, as an asperity passes a given point, can cause fatigue failure of material below the surface Theoretically wear particles are created by cracks from the surface spreading and moving upto the surface

5-Progressive tool wear under sliding conditions

Under sliding conditions, wear first occurs on the clearance or the flank face of the tool, in the form of a wear land due to rubbing against newly machined surface, as shown in Figure 1 1[1] The crater wear is formed some distance away from the cutting edge At high cutting speeds diffusion plays an important role Maximum temperature exists at some distance away from the cutting edge on the rake face and the crater formation initiates at this point. Figure 1 shows flank and crater wear.

6-Plasic deformation

The sharp cutting edge of the tool gets deformed and rounded off as a result of inadequate strength of the top edge A further flow of the work piece material over the flank surface changes the clearance angle, reducing it to zero or even negative for a certain portion of the flank Figure 1 2 [2] shows the tool wear by plastic deformation

## 1.2 Tool Wear Measurement

Worn cutting tools, if used in machining, can lead to dimensional instability of the work-piece, poor surface finish, increase in relative tool-work vibrations, increased overall production cost due to increased tool cost etc In this context, there is a need of a reliable and effective tool wear measuring sensor, to be developed

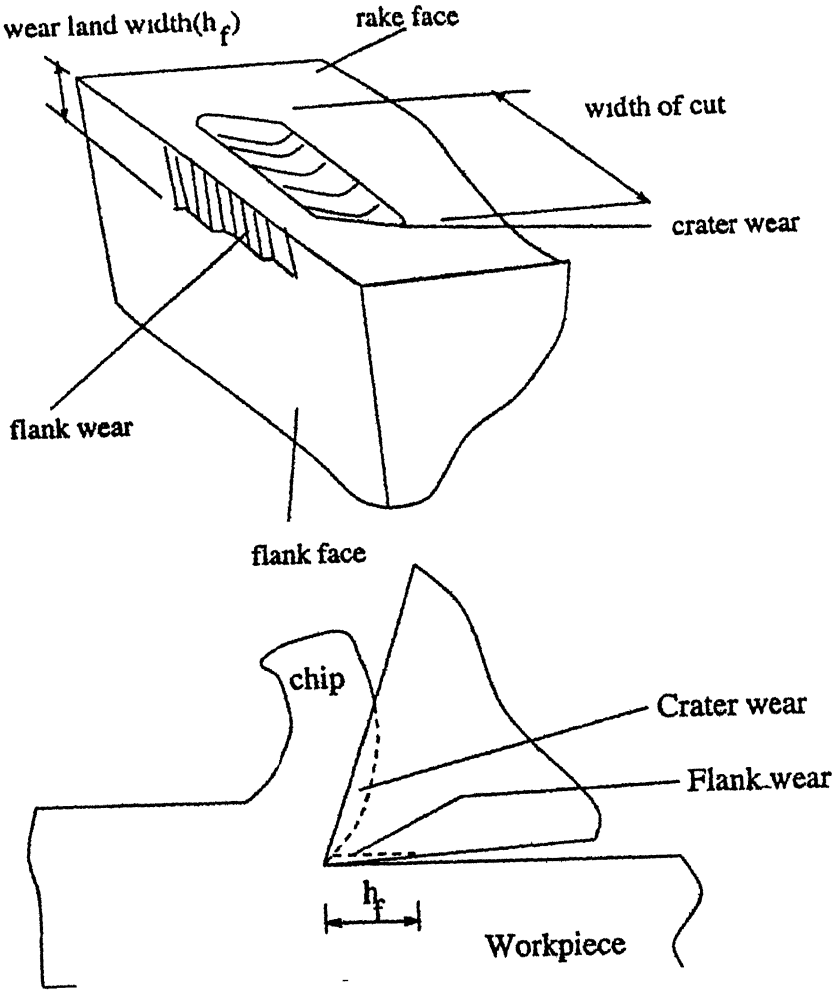


Figure 1.1: Tool wear [1].

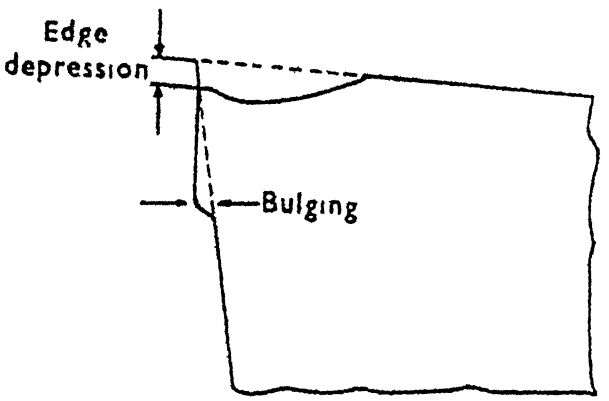


Figure 1.2: Plastic deformation [2].

The requirements of these sensors are

(i)-It should be rigid enough to be used in workshop environment
(ii)-It should be highly stiff and sensitive towards the input signals
(iii)-output should be quick and effective
(iv)-It should not be bulky so that it can be used on-line
(v)-It should be easily adaptable and cheap so that the cost of product does not increase

Sensing methods of the tool wear can be divided into direct or indirect measurements [3], the first method requires the measurement of a feature which is directly related to the tool wear Some of these sensors include electrical resistance, radioactive, optical, proximity and touch probs On the other hand indirect tool wear sensing employs the measurements of parameters which are indirectly related to the tool wear, some of those parameters are acoustic emission, cutting forces, vibrations, temperature and surface roughness

The reliability of these indirect methods depends on the accuracy and the robustness of the relationship between the tool wear and measured phenomena

## 1.3 Artificial Neural Network

Artificial Neural Networks (ANN) are biologically inspired, that is, they are composed of elements that perform in a manner that is analogous to the most elementary functions of the biological neurons. These elements are then organized in a way that may or may not be related to the analogy of the brain. Knowledge about the brain's overall operation is so limited that there is little to guide those who would emulate it. Hence, it is often necessary to go beyond current biological knowledge, seeking structures that performs useful functions Despite this superficial resemblance, ANNs exhibit a surprising number of brain's characteristics Their functions are often reminiscent of the human cognition

Biological neurons transmit electrochemical signals over neural pathways Each neuron receives signals from other neurons through special junctions called synapses Some inputs tend excite the neuron, while others tend to inhibit it. When the cumulative

effect exceeds a threshold value, the neuron fires, and sends a signal down to other neurons An artificial neuron simulates these simple biological characteristics Each artificial neuron receives a set of inputs Each input is multiplied by a weight analogous to synaptic strength The sum of all weighted inputs determines the degree of firing called the activation level and is further processed by an activation function which may be a threshold function or a smooth sigmoidal function

A neural network has a parallel distributed architecture with a large number of neurons and connections Each connection points from one node to another and is associated with a weight A simple viewing of the network structure and the behaviour is shown in Fig 1 3

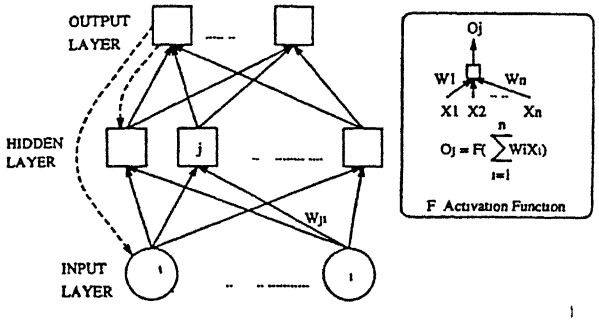


**Figure 1.3:The neural network computational model**

Construction of a neural network involves the following tasks [4]

- To determine the network properties consisting of network topology (connectivity), the type of connections, the order of connections, and the weight range
- To determine the node properties like the activation range and the activation function
- To determine the system dynamics, *i e*, the weight initialization scheme, the activation calculating formula and the learning rule

An artificial neural network can be considered as a network of many simple processors (units), each possibly having a small amount of local memory The units being connected by communication channels (connections) which usually carry numeric (as opposed to symbolic) data The units operate only on their local data and on the inputs, they receive via the connections The design motivation is what distinguishes neural networks from other mathematical techniques a neural network is a processing device, either an algorithm, or actual hardware whose design is motivated by the design and functioning of human brains and components thereof

There is no universally accepted definition of an Artificial Neural Network The following two are considered the best expressing the nature and the structure of the Artificial Neural Networks

- According to *DARPA* Neural Network study, a neural network is a system composed of many simple processing elements operating in parallel, whose function is determined by network structure, connection strengths and the processing performed at computing elements
- According to *Alexander*, a neural network is a massively parallel distributed processor that has a natural propensity for storing experimental knowledge and making it available for use It resembles the brain in two respects

    - Knowledge is acquired by the network through learning
    - Inter-neuron connection strengths known as synaptic weights are used to store the knowledge

Most neural networks have some sort of "training rule" whereby the weights of the connections are adjusted on the basis of presented patterns In other words, the neural networks" learn" from examples and exhibit some structural capabilities for generalization Learning is a process by which the free parameters of a neural network are adapted through a continuous process of stimulation by the environment in which the

network is embedded The type of learning is determined by the manner in which the parameter changes take place

The manner in which the neurons of the neural network are structured is intimately linked with the learning algorithm used to train the network In general, four different classes of network architectures are identified as [4]

- *Single layered feed forward networks* A layered network is a network of neurons organized in the form of layers In the simplest form of layered, there is only an input layer of source nodes that projects onto an output layer of neurons

- *Multi-layer feed-forward networks* These networks are distinguished by the presence of one or more hidden layers whose computation nodes are called hidden neurons By the presence of one or more hidden layers, the network is enabled to extract higher order statistics, as it requires a global perspective despite its local connectivity by virtue of extra set of synaptic connections and the extra dimension of the neural interaction

- *Recurrent networks* These networks have at least one feedback loop The presence of these feedback loops have a profound effect on the learning capabilities and on its performance

- *Lattice structures* A lattice consists of one or multidimensional array of neurons with a corresponding set of source nodes that supply input signals to the array These are actually feed-forward networks with the output neurons arranged in rows and columns

Based on the principle used by the network for learning, they can be broadly classified into two major categories

- *Supervised training* It requires the pairing of each input vector with a target vector representing the desired output Together these are called a training pair, usually a network is trained over a number of such training pairs An input vector is applied, the output of the network is calculated and compared to the corresponding desired vector and the difference is fed back through the network while weights are changed according to an algorithm that tends to minimize the error

- *Unsupervised learning* These are more plausible models of learning in the biological system They require no target vectors for the outputs, and hence, no comparisons to predetermined ideal responses The raining set consists solely of input vectors The training algorithm modifies network weights to produce output vectors that are consistent The training process, therefore extracts the statistical properties of the training set and groups similar vectors into classes

Neural networks solve problems by self-learning and self-organization They derive their intelligence from the collective behaviour of simple computational mechanisms at individual neurons

Computational advantages offered by neural networks include [5]

- Knowledge acquisition under the noise and uncertainty Neural networks can perform generalization, abstraction and extraction of the statistical properties from the data
- Flexible knowledge representation Neural networks can create their own representation by self-organization The network learns from examples by constructing an input- output mapping for the problem at hand They are inherently nonlinear in nature
- Efficient knowledge processing Neural networks can carry out computation in parallel Special hardware devices have been built which exploit this advantage

and thus, real time operation is feasible Training a network may be time consuming, but once it is trained it can operate very fast

- Fault tolerance Through distributed knowledge representation and redundant information encoding, the system performance degrades moderately in response to faults or errors

## 1.4 Literature Review

A lot of work has been done for the prediction of tool wear on line using neural networks A number of algorithms backed with experimental results were proposed by various research workers in the field of tool wear sensing with the help of neural network

*Dan et al* [3] provided a review of the numerous techniques and methods of monitoring tool wear particularly in the turning operations By and larger these techniques appear to be single minded,i e , they are capable of detecting and diagnosing tool wear and failure relating to particular classes of faults A universal approach, which can detect the very many failure modes in tool condition monitoring, has still not been investigated

*Masory* [6] proposed a wear model based on artificial neural network, which is used as pattern associator A network is trained to associate an input vector, consisting the readings of several different sensors for different input parameters, with an output vector consisting the actual tool wear measurement, by training process During operation, network is fed with sensors' readings, it fuses these data and provide estimated value of wear according to model established during training The estimation of tool wear obtained by this method is by far more accurate than the other methods, which use the same sensory inputs

*Lee et al* [7] used a neural network based approach for the prediction of the flank wear of the tool in turning as the wear prediction plays a important role in tip geometry compensation during precision machining They showed that by using force ratio, flank

wear can be predicted to within 8 to 11 9 % error and also by using force increment, flank wear can be predicted within 10 3 % of actual wear for various turning conditions

*Liu et al* [8] presented a multiplayer feed forward neural network algorithm for on-line monitoring of tool wear in turning operations, based on cutting conditions (speed and feed rate) and measured cutting force which are used as inputs to a three layer MLFF neural network, the network was first trained for various cutting conditions and then used to predict the tool wear for the cutting conditions different from those, used while training

*Choudhury et al* [9] developed an on-line monitoring system of tool wear in turning In this a Y shaped optical fiber sensor was used to sense the change in the dimensions of the work piece due to tool flank wear The signals from optical fiber are fed to the neural network program, which was trained earlier The neural network then predicts the tool wear

*Ghasempoor et al* [10] described a real time tool condition monitoring system for turning operations The system uses a combination of static and dynamic neural network with off-line and on-line training and cutting force components are used as diagnostic signals The system is capable of monitoring several wear components simultaneously However the accuracy of wear prediction is not same for all wear components

*Dimla Sr et al* [11] came up with a Neural Network based modular tool condition monitoring system for cutting tool state classification On-line cutting force and vibration data were acquired. Simultaneously the wear lengths on the cutting edges were measured, and these together with processed data were fed to a neural network trained to distinguish the tool state The system was found to be capable of accurate tool state classification in excess of 90% accuracy but deteriorated when the cutting conditions were significantly changed

*Dornfeld* [12] described the design and implementation of a neural network based system, combining the output of several sensors (acoustic emission, force and spindle motor current) for monitoring progressive tool wear in single point turning operation Multi-channel auto-aggressive series model parameters and power spectrum amplitude are used as inputs to the network The objective of the system is to extend the range of machining conditions over which the system performs successfully

*Leem et al* [13] proposed a customized Neural network for sensor fusion of acoustic emission and force in on-line monitoring of cutting tool wear Based on two critical concerns regarding practical and reliable tool wear monitoring systems, the maximum utilization of unsupervised sensor data and avoidance of off- line feature analysis, the neural network is trained by unsupervised Kohenen's Feature Map procedure followed by an input feature scaling algorithm After levels of tool wear are topologically ordered by Kohenen's feature map, input features of acoustic emission and force sensor signals are transformed via Input Feature Scaling so that the resulting decision boundaries of neural network approximate those of error minimizing Bayes classifier In a machining experiment, the customized neural network achieved high accuracy rates in the classification of levels of tool wear Also the neural network shows several practical and reliable properties for the implementation of monitoring system in manufacturing industries

*Purushothaman et al* [14] applied distributed neural network to the pattern recognition problem for classification of tool wear in a turning operation to discriminate between worn-out tool and a fresh tool A multi-layered perceptron with a back propogation algorithm has been used The network was trained off-line using 30 patterns each of six inputs Using the weights obtained during training, fresh patterns were tested, results for six fresh patterns were presented

*Li et al* [15] proposed that the use of discrete wavelet transform (DWT), which is much more efficient and just as accurate wa , may provide a realistic solution to the detection of tool breakage in o DWT used an analyzing wavelet

function, which is localized in both time and frequency to detect a small change in input signals They proposed a tool breakage monitoring system based on DWT of an acoustic emission and an electric feed current signal using an effective algorithm The experiment results show overall 98 5% reliability and the good real time monitoring capabilities of the proposed methodology for detecting tool breakage during drilling

*Dimla Sr et al* [16] described an on-line tool condition monitoring system, experimentally and analytically, involving the use of three mutually perpendicular components of cutting forces (static and dynamic) and vibration signature measurements The ensuing analysis in time and frequency domain showed some components of measured signals to correlate well to the occurred tool wear

*Uehara et al* [17] proposed a method based on an experimental fact that the pattern of the curve which shows the relationship between the cutting force (feed force) and the feed per revolution, is strongly influenced by the tool wear Due to increased rubbing at the cutting edge at small feed range, sudden rise or unstable fluctuation of the feed force was seen to reduce with the increase in crater wear. Measuring the peak height and the width of the flat part of the feed force oscillogram, the value of the flank wear and crater wear could be determined quantitatively This method was capable of detecting 0 15mm of flank wear and the 20μm of crater wear It was also capable of detecting chipping of the cutting tools, which causes an increase in feed force all over the feed range

*Koren, Danai and Ulsoy* [18] proposed a model-based approach to on- line tool wear and breakage detection under varying cutting conditions based on force measurements The standard recursive least square (RLS) algorithm, an on-line parameter estimation technique was used to estimate the unknown coefficients, the RLS algorithm ensured convergence of estimated error to zero The potential usefulness of this approach for separating the effect of feed variations and flank wear on force and in predicting tool failure due to excessive flank wear was illustrated Need for further research in on-line training of model-based approach using artificial intelligence methods was emphasized

*Kaye et al* [19] proposed a new technique for on-line prediction of the flank wear in turning using the spindle speed change An optical encoder mounted on the spindle shaft and interfaced to an IBM compatible microcomputer, was used as the speed-sensing element It is apparent that as the wear at the tool bit grows, the cutting force increases and the consequent torque increases on the spindle drive, causing a small reduction in spindle speed A mathematical model was developed which required the initial flank wear and only the changes in the spindle speed during cutting to predict the tool flank wear Surface response methodology was used to develop an empirical relation for determining the initial flank wear A low frequency sampling was initiated and electronically interrupted twice during machining process, during which time the sampling rate was increased A speed compensation factor was used to take care of the lathe transmission ratio, electrical configuration of the motor, and the torque speed relationship of the machine The method was capable of providing an almost continuous record of entire cutting process This method was able to predict any change in flank wear just before the tool breakage during the process

*Constantinides et al* [20] examined the use of spindle power for the estimation of the tool wear and the detection of end of effective tool life for a vertical milling machine Initially the raw data were analyzed using a FFT analyzer and the power spectrum was found Three parameters defined as the moving average, running means and cumulative sums were used to find the peak and the total power in frequency range. A considerable increase in the energy content of the power spectrum was seen when wear begins to increase A strong correlation was seen between the running mean of power and the running mean of wear rate Linear regression analysis supported the linear relationship between the cumulative sum of power spectral energies and the total flank wear The residual obtained by computing a least square linear fit to the plot of cumulative sum against cutting time clearly indicates the onset of high wear region The results show that it could be the basis of a simple method, despite requiring computations, for on-line detection of the tool wear

*Danai and Ulsoy* [21] proposed a dynamic state model for the design of an adaptive observer for the tool wear estimation in turning based on force measurements Using the

relationships available in the literature, a non-linear model was developed with the flank wear and the crater wear as the state variables , cutting force as the output and the feed as the input The model was linearized about an operating point along its trajectory and Eigen analysis was performed to check its suitability and stability For particular cutting conditions, this provides the model structure, which together with an on-line parameter estimation technique could be used as an on-line wear estimator

*Lim* [22] investigated the influence of the cutting conditions on the measured vibration signals, and developed a strategy for detecting the tool wear The analysis of the vibration signals was done using an accelerometer, charge amplifier and a FFT analyzer Experimental results with different cutting conditions (varying speed, feed and depth of cut) were reported as acceleration vs flank wear curves, using a calibration graph from the spectrum plots These curves clearly showed that during the turning process, the acceleration amplitude constantly produced two peaks during the life of the tool The increase in the vibration signals was attributed to the increasing friction at the tool-work piece interface The initial drop was reported to be due to the considerable increase in the friction due to the tool wear It was suggested that this twin peak signal can be incorporated in a software program to indicate the onset of a tool failure A test routine would first monitor the onset of the tool failure by evaluating the percentage drop from second peak as the criterion for implementing the necessary tool change automatically The experimental results were compared with the simulation model of Danai and Ulsoy [21] and a good agreement (with an error of only 3 6 %) was found The tool life as a function of variable amplitude was also established

*Choudhury et al* [23] described a system which deals with on-line tool wear sensing and the development of a feed back control system to provide compensation for the tool wear to keep the dimensions of the work-piece within tolerance limits An optical displacement sensor was used for on-line monitoring of the tool wear The proposed device for control is quite simple and can be used in an industrial environment

*Fan and Chao* [24] developed a new technique for in-process work-piece dimensional measurements and error compensation in turning During operation the diameter was obtained through three servo measurement units Each unit is composed of a non-contact proximitor for direct gap sensing, a stepping motor controlled linear carriage to move the proximitor for surface tracing, and a LVDT for position feedback of the carriage The error compensation strategy was implemented by interrupting a compensator in the position feedback loop of the NC servo system so that the tool position could be directly controlled by an external personal computer Experimental results show that the accuracy of the work-piece can be maintained within reasonable tolerance regardless of the length and shape being machined

*Sanjanwala et al* [25] observed the dimensional inaccuracies as one of the major problems during the turning of a long bar This is explained by the fact that the flank wear on the tool causes a tapering effect They described the design and the testing of a pneumatic feedback system that can be mounted on a centre lathe to improve the dimensional stability during turning by on-line tool wear sensing and compensation The proposed system consists of a pneumatic sensor to sense the wear during machining, a pilot controlled direction control valve to amplify the signal obtained from the pneumatic sensor and an actuating mechanism to move the tool for compensation of the dimensional inaccuracies The proposed system was tested for various cutting conditions The improvement in dimensional accuracy is shown by taking a cut with a pneumatic feedback system and then repeating the cut with identical cutting conditions, but without feedback The results show that the use of proposed feedback system results in improved dimensional accuracy

*Muttur* [31] indirectly monitored the flank wear by measuring the temperature generated during turning Experiments were conducted using HSS tool and tungsten carbide tool bits and EN-24 work piece. Rotational speed, feed and the depth of cut were used as the three input parameters Empirical relation between the temperature and the input parameters as well as between the flank wear land and the input parameters have been established Experimental values of temperature and flank wear land have been compared

with theoretical values The temperature generated at the flank has been assumed to be approximately 4% of the total temperature and this is related to the flank wear land

For on line monitoring of the tool wear under varying cutting conditions, Artificial Neural Network (ANN) can approximate continuous non-linear functions well and it is based on the mathematical principles and model for biological neurons and the nervous system, ANN has following features universal approximating, parallel distributed processing, hardware implementation, learning and adaptation, multi-variable systems These features are the advantages for the tool wear monitoring

From the above research works, it is clear that a reliable and effective on-line monitoring sensor for tool wear has an important role to play in realization of above concepts In the absence of any standard model to predict the tool wear for a variety of materials, operating conditions and tooling, sensing technology will play the most important role in factories of future

## 1.5 Objective of the present work

Although a lot of work have been done for the prediction of tool wear by using Neural Network and other mathematical methods like design of experiment etc, but very few work has been done for the comparison among the various methods of tool wear prediction

In the present work the result of the tool wear, surface finish and temperature predictions by Neural Network and Design of Experiment are compared to find out which method gives more realistic predictions (nearer to the measured ones)

The objectives of the present work are

(i) Tool wear, surface finish and temperature predictions with the help of Design of Experiments

(ii) Prediction of the above response variables with the help of Neural Network.

(iii) Comparison between the results from the above two prediction methods

(iv) To find out more reasonable methods with realistic results out of above two methods

Here the training data for the Neural Network program are taken in such a way so that it cover ranges for all input parameters, and also the same data may be used to find out a regression equation between tool wear and the input parameters, when using design of experiments

## 1.6 Organization of thesis

The thesis consists of various chapters,

Chapter 2 Covers the theoretical aspects such as Artificial Neural Network and Design of Experiment

Chapter 3 is experimental setup and procedure, which consists of experimental setup and details of components required for experimental setup

Chapter 4 is results and discussion This chapter consists of the experiments conducted to

- Predict different response variables i e the tool wear, cutting zone temperature and surface roughness, with the help of Neural Network and Design of Experiment
- Compare the two results with the measured values of the responses, to find out the more realistic approach for tool wear prediction

Chapter 5· Conclusion of thesis work has been drawn and scope for the future work has been elaborated

| | *Procedure* | *Measurement* | *Transducer* |
|---|---|---|---|
| *Direct* | Optical | Shape or position of the cutting edge | TV camera, optical transducer |
| | Wear particles and radioactivity | Particle size and concentration, radioactivity activity | Spectrophotometer, scintillator |
| | Tool/work junction resistance | Change of junction resistance | voltmeter |
| | Work-piece size | Dimensions of the work-piece | Micrometer, optical, pneumatic, ultrasonic, electromagnetic transducers |
| | Tool/work distance | Distance of work-piece and tool or tool holder | Micrometer, pneumatic gauge, displacement transducers |
| *Indirect* | Cutting force | Change of cutting force | Dynamometer, strain gauges |
| | Acoustic emission | Stress wave energy | AE transducer |
| | Sound | Acoustic waves | Microphone |
| | Vibration | Vibration of tool and/or tool posts | Accelerometer |
| | Temperature | Variation of cutting temperature on tool | Thermocouple, pyrometer |
| | Power input | Power or current consumption of spindle or feed motor | Ampere meter |
| | Roughness of machine surface | Changes in surface roughness of the work-piece | Mechanical stylus, optical transducer |

Table 1 Principal classifications of tool wear sensing methods [3]

# *Chapter- 2*

# Theoretical Aspects and Analysis

## 2.1. Planning of experiment

A scientific approach to planning of experiments must be incorporated in order to perform an experiment most effectively Statistical design of experiments is the process of planning the experiments so that the appropriate data could be collected which may be analyzed by statistical method resulting in valid and objective conclusions

Planning of experiments was employed in order to fulfill the following requirements

- To get the data uniformity distributed over the whole range of controllable factors to be investigated
- To reduce the total number of experiments
- To establish a relationship between different input variables and the output accurately in the selected range of investigation

### 2.1.1: $3^k$ factorial design for three factors

$3^k$ factorial design is the most widely used factorial design having three levels for each of 'k' factors The three levels of factors are referred to as low (0), intermediate (1) and high (2)

If there are three factors (say A, B and C) under study and each factor is at three levels arranged in a factorial experiment, then, this constitutes a *$3^3$ factorial design.* The experimental layout and treatment combination notations are shown in Figure 3 1

The 27 treatment combinations have 26 degrees of freedom Each main effect has two degrees of freedom, each two factor interaction has 4 degree of freedom. If there are n

replicates, then there are $n \times 3^3 - 1$ degrees of freedom and $3^3(n\text{-}1)$ degrees of freedom for error[27]

In the present experimental work, there are 3 input variables which are cutting speed, feed and depth of cut All the three levels of these parameters are decided on the basis of

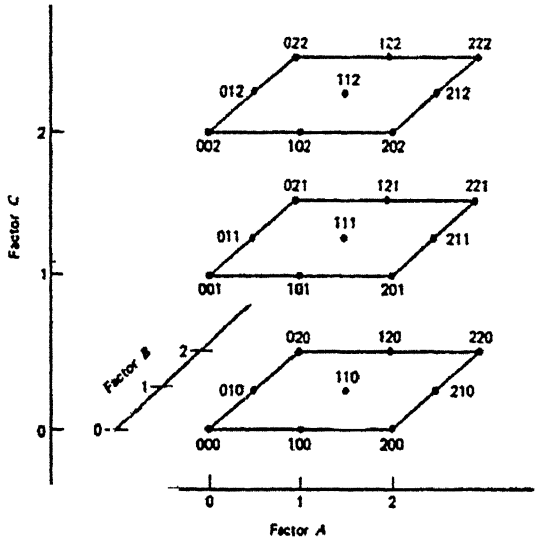


Figure 2 1 Treatment combinations in a $3^3$factorial design[27]

handbooks [28], machine capabilities and experience. The levels of all three factors are given in table 2

| Cutting speed (m/min) | Feed (mm/rev) | Depth of cut (mm) |
|---|---|---|
| 20 | 0 075 | 0.4 |
| 27 5 | 0 1 | 0 6 |
| 35 | 0.125 | 0.8 |

Table 2 Different levels of cutting parameters

## 2.1.2: Simple linear regression

If a relationship between single variable $x$ and a response variable $y$ is to be determined, the variable x is generally assumed to be controllable by the experimenter Suppose the true relationship between $y$ and $x$ is a straight line, and that the observation $y$ at each level of $x$ is a random variable Then expected value of $y$ for each value of $x$ [$E(y/x)$] is, [27]

$$E(y \mid x) = \beta_0 + \beta_1 x \qquad (2.1)$$

where the parameters $\beta_0$ and $\beta_1$ are the unknown constants It is assumed that for each

observation $y$ can be described by the model as

$$y = \beta_0 + \beta_1 x + \varepsilon \qquad (2.2)$$

where $\varepsilon$ is a random error with mean zero and variance, $\sigma^2$ The regression model (2.2) involving only single regressor variable $x$, is called simple linear regression model

If 'n' number of data points are obtained through experimentation, then $\beta_0$ and $\beta_1$ can be estimated by least squares The least square function is

$$L = \sum_{j=1}^{n} \varepsilon_j^2 = \sum_{j=1}^{n} [y_j - \beta_0 - \beta_1 x_j]^2 \qquad (2.3)$$

Minimization of least squares is simplified if the model is rewritten as

$$y = \beta_0' + \beta_1 (x - \bar{x}) + \varepsilon \qquad (2.4)$$

where,

$\bar{x} = (\frac{1}{n}) \sum_{j=1}^{n} x_j$ and $\beta_0' = \beta_0 + \beta_1 \bar{x}$ here repressor variable is corrected for its average

Thus least squares function becomes

$$L = \sum_{j=1}^{n} [y_j - \beta_0' - \beta_1 (x_j - \bar{x})]^2 \qquad (2.5)$$

The least square estimators of $\beta_0'$ and $\beta_1$, say $\hat{\beta}_0'$ and $\hat{\beta}_1$ must satisfy,

$$\frac{\partial L}{\partial \beta_{\circ}'}\Big|_{\hat{\beta}_{\circ}',\hat{\beta}_1} = -2\sum_{j=1}^{n}[y_j - \hat{\beta}_{\circ}' - \hat{\beta}_1(x_j - \bar{x})] = 0$$

$$\frac{\partial L}{\partial \beta_1}\Big|_{\hat{\beta}_{\circ}',\hat{\beta}_1} = -2\sum_{j=1}^{n}[y_j - \hat{\beta}_{\circ}' - \hat{\beta}_1(x_j - \bar{x})](x_j - \bar{x}) = 0$$

Simplifying above two equations, we get,

$$n\hat{\beta}_{\circ}' = \sum_{j=1}^{n} y_j$$

$$\hat{\beta}_1 \sum_{j=1}^{n}(x_j - \bar{x})^2 = \sum_{j=1}^{n} y_j(x_j - \bar{x}) \qquad (2\,6)$$

These are the least square normal equations Their solution is,

$$\hat{\beta}_{\circ}' = \frac{1}{n}\sum_{j=1}^{n} y_j = \bar{y} \qquad (2\,7)$$

$$\hat{\beta}_1 = \frac{\sum_{j=1}^{n} y_j(x_j - \bar{x})}{\sum_{j=1}^{n}(x_j - \bar{x})^2} \qquad (2\,8)$$

Thus, $\hat{\beta}_{\circ}'$ and $\hat{\beta}_1$ are the least squares estimators of intercept and slope respectively

The fitted linear regression model is,

$$\hat{y} = \hat{\beta}_{\circ}' + \hat{\beta}_1(x - \bar{x}) \qquad (2\,9)$$

For convenience, symbols can be used for numerator and denominator of equation (2 8)

$$S_{xx} = \sum_{j=1}^{n}(x_j - \bar{x})^2 = \sum_{j=1}^{n} x_j^2 - \frac{(\sum_{j=1}^{n} x_j)^2}{n} \qquad (2\,10)$$

$$S_{xy} = \sum_{j=1}^{n} y_j(x_j - \bar{x}) = \sum_{j=1}^{n} x_j y_j - \frac{(\sum_{j=1}^{n} x_j)\,(\sum_{j=1}^{n} y_j)}{n} \qquad (2\,11)$$

$S_{xx}$ is called corrected sum of squares of $x$ and $S_{xy}$ is called corrected sum of cross products of $x$ and $y$ using these notations, the least square estimator of slope is

$$\hat{\beta}_1 = \frac{S_{xy}}{S_{xx}} \qquad (2.12)$$

## 2.1.3: Fitting Response Surface

If all the factors represent quantitative variables, then response y, can be represented as a function of the levels of variables [29]

$$y_u = \phi(x_{1u}, x_{2u}, \ldots, x_{ku}) + e_u \qquad (2\ 13)$$

Where, u=1,2,3 N represents the N observations in the factorial experiment and $x_{iu}$ represents the level of $i^{th}$ factor on the $u^{th}$ observation $e_u$ is the experimental error of the $u^{th}$ observation the function $\phi$, is called Response Surface These experimental designs can be developed for fitting first or second order designs

The fitting polynomials can be treated as a particular case of Multiple Linear Regression The relation between $y_u$ and $x_{iu}$ is of the form.

$$y_u = \beta_0 x_{0u} + \beta_1 x_{1u} + \ldots + \beta_k x_{ku} + e_u \qquad (2\ 14)$$

where k is the total number of variables The two-way array of $x_{iu}$ is called the X matrix and the column vetor of $y_u$ is called Y vector

The least square estimates of $b_i$ of the $\beta_i$ are chosen so as to minimize the sum of the squares of deviations

$$\sum_{u=1}^{N} (y_u - b_0 x_{0u} - b_1 x_{1u} - \ldots - b_k x_{ku})^2 \qquad (2\ 15)$$

The value of $b_i$ which minimizes this expression, satisfies the normal equations which are obtained as

| (ij) | | (iy) |
|---|---|---|
| 00 01 | 0k | (0y) |
| 10 11 | 1k | (1y) |
| | | . |
| | | . . |
| k0 k1 | kk | (ky) |

where,

$$(ij) = (ji) = \sum_{u=1}^{N} x_{iu} x_{ju} = \text{Sum of products of } i^{th} \text{ and } j^{th} \text{column in X matrix}$$

$$(ii) = \sum_{u=1}^{N} x_{iu}^2 = \text{Sum of squares of } i^{th} \text{ column in X}$$

$$(iy) = \sum_{u=1}^{N} x_{iu} y_u = \text{Sum of products of the } i^{th} \text{ column in X and Y} \qquad (2\ 16)$$

From the above normal equation matrix $c_{ij}$ ,inverse matrix of the matrix (ij) is obtained

$$c_{ij} = (X'X)^{-1}$$

$$\begin{matrix} c_{00}\ c_{01} \ldots\ldots\ldots c_{0k} \\ c_{10} c_{11} \ldots\ldots\ldots c_{1k} \\ c_{20} c_{21} \ldots\ldots\ldots c_{2k} \\ \ldots\ldots\ldots\ldots\ldots\ldots \\ \ldots\ldots\ldots\ldots\ldots\ldots \\ c_{k0}\ c_{k1} \ldots\ldots\ldots c_{kk} \end{matrix}$$

Thus the regression coefficients $b_i$ can be obtained as

$$b_i = \sum_{j=0}^{k} c_{ij} (jy) \qquad (2\ 17)$$

= Sum of products of the $i^{th}$ column of the $c_{ij}$ with the column $(jy)$

## 2.2 The Neural Network

In this section the design and working of the feed forward three layered artificial neural network used in present work, is explained Typically, these networks consist of a set of source nodes (sensory units) that constitute the input layer, one or more hidden layer of the computation nodes and an output layer of computation nodes The input signal propagates through the network in the forward direction on a layer-by-layer basis The feed forward connections in the network implies the absence of any recurrent or feedback connections The neural networks are usually referred to as the multi-layer perceptrons

Multi-layer perceptron have been applied successfully to solve some difficult and diverse problems by training them in a supervised manner with highly popular algorithm known as the error back propagation algorithm This algorithm is based on the error-correction learning rule A multi-layer perceptron has three distinctive characteristics

- The model of each neuron in the network includes a smooth nonlinearity at the output end The presence of nonlinearities is important because otherwise the input output relation of the network could be reduced to that of a single layer perceptron, which seriously complicates many of the problems
- The network contains one or more layers of hidden neurons that are not the part of the input and output of the network These hidden neurons enable the network to learn complex tasks by extracting progressively more meaningful features from the input patterns
- The network exhibits a high degree of connectivity, determined by the synapses of the network

The development of the back propagation algorithm represents a landmark in the history of neural networks in the way that it provides a computationally

efficient method for the training of the multi-layer perceptron A multi-layer perceptron trained with the back propagation algorithm may be viewed as a practical way of performing a non-linear input-output mapping of a general nature These are known to be used as universal approximator In the current application, the objective is to use the network to learn mapping between input and output patterns The components of the input pattern consist of the control variables of the machining operation (the cutting speed, feed, depth of cut), whereas the output pattern components represent the measured factors (roughness value and wear) and response from sensors (temperature) The nodes in the hidden layer are necessary to implement the nonlinear mapping between the input and output patterns

Each neuron is connected to all the other neurons in the adjacent layer through the weighted connections In the forward pass, the synaptic weights remain unaltered throughout the network and the function signals of the network are computed on a neuron-by-neuron basis Specifically, the function signal appearing at the output of neuron, $j$, is computed as

$$y_j(n) = \Phi(v_j(n)) \qquad (2\ 18)$$

Where $v_j$ (n) is the net internal activity level of neuron, $j$, defined by

$$v_j(n) = \sum_{i=0}^{p} w_{ji}(n) y_i(n) \qquad (2\ 19)$$

Where $p$ is the total number of inputs applied to the neuron, $i$, and $w_{ij}(n)$ is the synaptic weight connecting neuron, $i$, to neuron, $j$, and $y_i(n)$ is the input signal of neuron, $j$ or, equivalently, the function signal appearing at the output of neuron, $i$. If the neuron, $i$, is in the first hidden layer of the network, then the index, $i$, refers to the $i^{th}$ input terminal of the network, for which we write

$$y_i(n) = x_i(n) \qquad (2.20)$$

Where $x_i(n)$ is the $i^{th}$ element of the input pattern If, on the other hand, neuron $i$ , is in the output layer of the network, the index, $i$, refers to the $i^{th}$ output terminal of the network, for which we write

$$y_i(n) = z_i(n) \qquad (2.21)$$

Where $z_i(n)$ is the $i^{th}$ element of the output pattern This output is compared to the desired response, $d_i(n)$, for obtaining the error signal for the $i^{th}$ output neuron Thus forward pass begins with presenting the input pattern at the input layer and ends with finding the error signal for each neuron at output

The backward pass starts at the output layer by passing the error signals left-ward through the network, layer-by-layer, and recursively calculating the local gradients, $\delta$, for each neuron This recursive process permits the synaptic weights of the network to undergo changes in accordance with the delta rule as discussed in the next section. For a neuron located in the output layer, the $\delta$, is simply equal to the error signal of that neuron multiplied by the first derivative of this non-linearity. In this way we calculate the changes in the weights of all the connections feeding into the output layer Using the $\delta$ for the neurons in the output layer, $\delta$ for the neurons in penultimate layer and thus the change of weights of all connections feeding into it can be calculated The recursive computation is further continued, layer-by-layer, by propagating the changes to all synaptic weights made.

In the back propagation algorithm, we approximate the trajectory in the weight space computed by the steepest descent method The value of the learning rate constant $\eta$ is to be decided before starting the learning process When a smaller value is used, the changes to the synaptic weights in the network will also be smaller and the trajectory in the weight space will be smoother This, however, results in the slower rate of learning And if a higher value of $\eta$ is used, the resulting changes in the synaptic weights assume such a form that the network may become unstable A simple and decent method of increasing the learning rate and at the same time avoiding the instability is, by introducing an extra term in the equation for finding the changes in weights as

$$\Delta w_{ij}(n) = \alpha \Delta w_{ij}(n-1) + \eta \delta_j(n) y_j(n) \qquad (2\ 22)$$

Where α is the momentum constant The use of the momentum constant is known to provide beneficial effects on the learning behaviour of the network It may also prevent the learning process from terminating in the shallow local minima on the error surface

During the training process of the network, the set of training data is presented to the network in a epoch-by-epoch basis One complete presentation of the entire training set to the network is called epoch For a given training set, this may proceed in either the pattern mode or the batch mode of learning In the pattern mode, weight updating is performed after the presentation of each training example This is indeed the mode of operation for which the back propagation algorithm was developed In the batch mode, the weight updating is performed after the presentation of all the training examples that constitute an epoch For a particular epoch, the cost function is defined as the sum of squared errors as

$$E(n) = \sum_{n=1}^{N} \sum_{j=1}^{r} e_j^2(n) \qquad (2\ 23)$$

Where, $e_j(n)$ is the error signal The inner summation is performed over all the neurons in the output layer, while the outer summation is performed over entire training set When compared, pattern mode is found to require less local storage for each synaptic connection and also helps the network from being trapped in the local minima However, the batch mode is known to provide a more accurate estimate of the gradient vector

In the present work, another method known as the *active learning* is used During the training process, initially all patterns in the training set are presented to the network and the corresponding error parameter (sum of squared errors over the neurons in the output layer) is found for each of them Then the pattern with the maximum error is found and this is used for changing the synaptic weights Once the weights are changed, all the training patterns are again fed to the network and the pattern with the maximum error is then found This process is continued till the maximum error in the training set becomes less than the allowable error specified by the user This method has the advantage of avoiding a large number of

computations, as only the pattern with the maximum error is used for changing the weights This method also avoids the problem known as thrashing (when weights are changed using a particular pattern from the training data, the error for some other pattern may change to a higher value than the allowable value In other words, training on $E^{(p)}$ can cause unlearning on $E^{(q)}$ for $p \neq q$ this problem is known as trashing )

It is proposed in literature [5] that a multiplayer perceptron trained with the back propagation algorithm may learn faster when the sigmoidal activation function used, is asymmetric than when it is non-symmetric In the present work, a popular asymmetric nonlinear function, known as the hyperbolic tangent, is used The use of this activation function requires a small modification in the standard Back-propagation algorithm, which uses the logistic function

$$\Phi(x) = a \tanh(bx)$$

$$= a \left(\frac{1-e^{-bx}}{1+e^{-bx}}\right)$$

$$= \left(\frac{2a}{1+e^{-bx}} - a\right) \qquad (2\ 24)$$

Where a = 1 716 and b =0 667

## 2.2.1 Derivation Of Back Propagation Algorithm [5]

The error signal at the output of the neuron, $j$, at iteration, n, is defined as

$$e_j(n) = d_j(n) - y_j(n) \qquad (2\ 25)$$

The sum of squared errors is obtained as

$$E(n) = \frac{1}{2}\sum_{j=1}^{r} e_j^2(n) \qquad (2\ 26)$$

Where $r$ is the number of neuron in the output layer

Consider a neuron, $j$,fed with the signal produced by the preceeding layer of neurons The net internal activity level, $v_j(n)$, produced at the neuron, $j$, is therefore

$$v_j(n) = \sum_{i=0}^{p} w_{ji}(n) y_i(n) \qquad (2\ 27)$$

Where $p$ is the number of inputs fed to the neuron, $j$ Hence

$$y_j(n) = \Phi(v_j(n)) \qquad (2\ 28)$$

In the Back propagation algorithm, a correction, $\Delta w_{ji}(n)$, is applied to the synaptic weights which is proportional to the instantaneous gradient This gradient can be expressed as

$$\frac{\partial E(n)}{\partial w_{ji}(n)} = \frac{\partial E(n)}{\partial e_j(n)} \frac{\partial e_j(n)}{\partial y_j(n)} \frac{\partial y_j(n)}{\partial v_j(n)} \frac{\partial v_j(n)}{\partial w_{ji}(n)}$$

from eq 2 26,

$$\frac{\partial E(n)}{\partial e_j(n)} = e_j(n)$$

from eq 2 25,

$$\frac{\partial e_j(n)}{\partial y_j(n)} = -1$$

from the eq.2 28,

$$\frac{\partial y_j(n)}{\partial v_j(n)} = \phi'(v_j(n))$$

and from eq 2 27,

$$\frac{\partial v_j(n)}{w_{ji}(n)} = y_i(n)$$

Therefore,

$$\frac{\partial E(n)}{\partial w_{ji}(n)} = -e_j(n)\phi'(v_j(n))y_i(n)$$

The correction applied to the synaptic weights, $w_{ji}(n)$ is given by delta rule as

$$\Delta w_{ji}(n) = -\eta \frac{\partial E(n)}{\partial w_{ji}(n)}$$

Where $\eta$ is the learning rate parameter Therefore,

$$\Delta w_{ji}(n) = -\eta \delta_j(n) y_i(n)$$

Where the local gradient,

$$\delta_j(n) = e_j(n)\phi''(v_j(n)) \qquad (2\ 29)$$

As the activation function used, is the hyperbolic tangent, we have

$$\phi(v_j(n)) = a\tanh(bv_j(n))$$

$$= a\frac{1-\exp(-bv_j(n))}{1+\exp(-bv_j(n))}$$

$$= \frac{2a}{1+\exp(-bv_j(n))} - a$$

$$\Rightarrow \phi'(v_j(n)) = \frac{2ab\exp(-bv_j(n))}{(1+\exp(-bv_j(n)))^2}$$

$$\Rightarrow \phi'(v_j(n)) = \frac{2ab}{(1+\exp(-bv_j(n))}\left\{1-\frac{1}{(1+\exp(-bv_j(n))}\right\}$$

$$= b\{a+\phi(v_j(n))\}\left\{1-\frac{a+\phi(v_j(n))}{2a}\right\}$$

$$= \frac{b}{2a}(a+\phi(v_j(n)))(a-\phi(v_j(n)))$$

$$= \frac{b}{2a}\{a^2-\phi^2(v_j(n))\}$$

$$= \frac{b}{2a}\{a^2-y_j^2(n)\} \qquad (2\ 30)$$

In the eq 2 25, the $e_j(n)$, is straight forwardly known for the output layer neurons But for the hidden layer neurons, this term is to be determined recursively in terms of the error signals of all the neurons to which it is connected

From the eq 2 29,

$$\delta_j(n) = -\frac{\partial E(n)}{\partial y_j(n)} \frac{\partial y_j(n)}{\partial v_j(n)}$$

$$= -\frac{\partial E(n)}{\partial y_j(n)} \phi'(v_j(n))$$

From the eq 2 26,

$$\frac{\partial E(n)}{\partial y_j(n)} = \sum_k e_k \frac{\partial e_k(n)}{\partial y_j(n)}$$

$$= \sum_k e_k \frac{\partial e_k(n)}{\partial v_k(n)} \frac{\partial v_k(n)}{\partial y_j(n)}$$

but since

$$e_k(n) = d_k(n) - y_k(n) = d_k(n) - \phi(v_k(n))$$

We have,

$$\frac{\partial e_k(n)}{\partial v_k(n)} = -\phi'(v_k(n))$$

and since

$$v_k(n) = \sum_{j=0}^{q} w_{kj}(n) y_i(n)$$

$$\Rightarrow \frac{\partial v_k(n)}{\partial y_j(n)} = w_{kj}(n)$$

Therefore,

$$\frac{\partial E(n)}{\partial y_j(n)} = -\sum e_k \phi_k'(v_k(n)) w_{kj}(n)$$

$$= -\sum \delta_k(n) w_{kj}(n)$$

Hence, the local gradients for the hidden layer neurons can be written as

$$\delta_j(n) = \phi_j'(n)(v_j(n)) \sum_J \partial_k(n) w_{kj}(n)$$

$$= (\frac{b}{2a})(a^2 - y_i^2(n)) \sum_J w_{jk}(n) \delta_k(n) \qquad (2\,31)$$

Summarizing, the relations developed may be written as

- The correction $\Delta w_{ji}(n) =$ (learning rate parameter, $\eta$) x (local gradient, $\delta$) x (input signal of neuron $j, y_j(n)$)
- For the output layer neurons,

$$\delta_j(n) = \frac{b}{2a}(a^2 - y_i^2(n)) e_j(n)$$

- For the hidden layer neurons,

$$\delta_j(n) = \frac{b}{2a}(a^2 - y_i^2(n))(\sum_k w_{kj}(n) \delta_k(n)$$

Figure2 2 shows the flowchart of the software developed

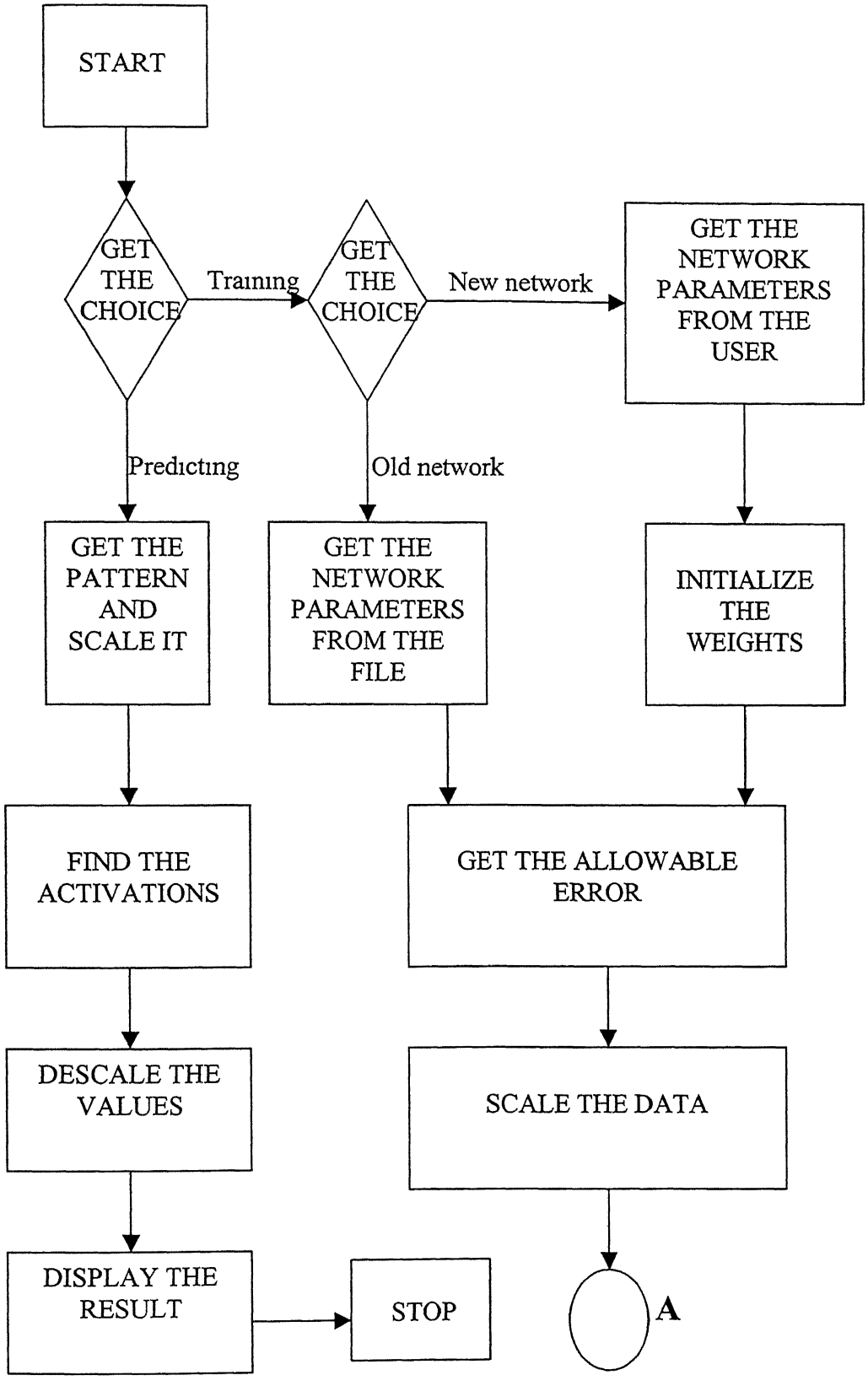
START
GET THE CHOICE
Training
GET THE CHOICE
New network
GET THE NETWORK PARAMETERS FROM THE USER
Predicting
Old network
GET THE PATTERN AND SCALE IT
GET THE NETWORK PARAMETERS FROM THE FILE
INITIALIZE THE WEIGHTS
FIND THE ACTIVATIONS
GET THE ALLOWABLE ERROR
DESCALE THE VALUES
SCALE THE DATA
DISPLAY THE RESULT
STOP
A

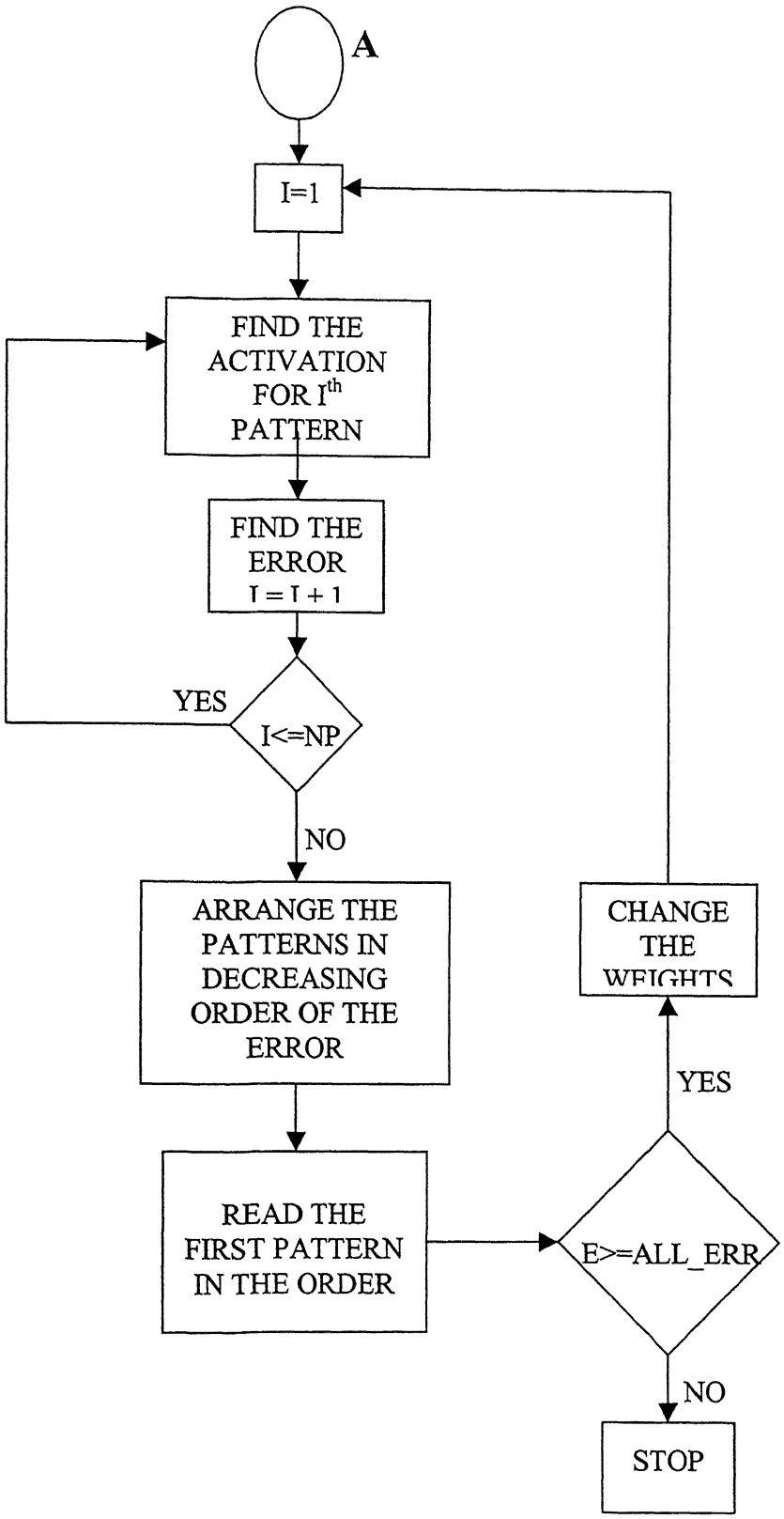


Fig 2 2 Flowchart for the Neural Network program

## 2.3 Optical Sensor System

The basic idea that the surface finish of a reflecting surface dictates the amount of reflected light from a light source, is used to develop an optical sensor for the monitoring of the tool wear It is known that the flank wear on the cutting tool is responsible for surface roughness of the parts produced Thus with the wear on the tool increasing, the surface finish of the work-piece will be deteriorating continuously If a light source is moved parallel to the axis of work-piece while turning, keeping the distance between them constant, the intensity of the reflected light can be sensed and the tool wear can be correlated to the change in light intensity This is believed [23] to provide a simple yet reliable tool wear sensor The basic components of the optical sensor system include the optical fiber transducer, the sensing and amplification circuit and a recorder to measure the signals

### 2.3.1 Optical Fiber Transducer

The advent of efficient and cost effective optical fiber technology for telecommunication requirements resulted in the development of a new generation physical measurement transducers. The fiber optics transducers are generally classified as intensity modulated, interferomatric, polarization-based and wavelength modulated devices. Of these, intensity modulated devices are the commonly used ones. They are either reflective or transmissive, and can be operated in on-off or proportional mode Most of the fiber optic transducers use basically some form of the optical lever principle (a means of detecting small displacements by reflected beam of the light from the object) Figure 2 3 shows the cross-section of a step index multimode fiber [26] These fibers are made of a cylindrical core, typically 50 micrometer in diameter, surrounded by a cladding whose reflective index is less than that of core The numerical aperture of the fiber in the air is given as $$NA = sin\theta_c = \sqrt{n_1^2 - n_2^2}$$

Where $n_1$ and $n_2$ are the reflective indices of the core and the cladding material respectively and $\theta_c$ is the angle of incidence at the core-cladding interface at the critical angle for the total internal reflection The input ray consequently propagates along the fiber with no reflection losses

Another important parameter of the optical fiber transducer is the spatial resolution also known as the distance resolution. In the optical time domain reflectometer (OTDR), a rating based on the shortest distance along the length of an optical wave-guide (as an optical fiber) that the OTDR can distinguish on its display screen (usually CRT) is called the spatial resolution It is the measure of how close together the two events or faults can be distinguished as separate events

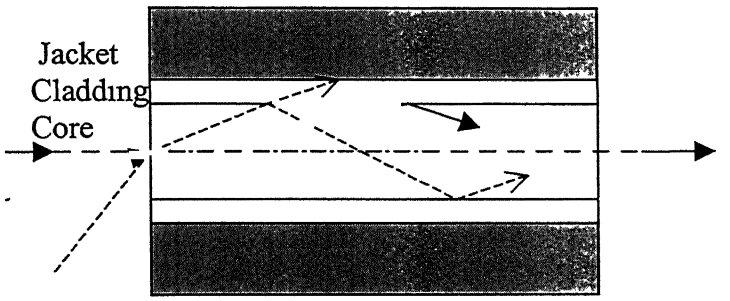


Fig 2 3 Sectioned view of a step index multimode fiber [26]

Usually the sensor consists of a bifurcated fiber bundle with one leg connected to a photodetector and the other to a light source (preferably monochromatic) At the face of merger of the two bundles the fibers from the two legs are randomly mixed Other configurations with hemispherical or the concentric- transverse-inside fiber grouping are also available

The basis for the operating mechanism is the interaction between the source and the field of view of the detector fibers A simplified illustration of this effect is shown in Figure 2.4 At contact or zero gap, the whole amount of light passes through the source fibers, strikes the work-piece surface and is reflected back into

the same source fibers, almost no light get reflected into the sensing fibers and hence produces zero output voltage An increase in the probe to target distance will result in some reflected light being captured by the receiving fibers, so we put the optical sensor at some distance form the work piece surface Depending upon the surface finish of the job the intensity of the light captured by the receiving fibers will increase or decrease (scattering effect) As an optical fiber has an aperture, that is, an angle beyond which the rays are neither nor transmitted, there will be a preferred stand-off distance at which the light intensity from the transmitting fibers to the receiving fibers reflected from the surface, will be maximum As the sensor is placed further back, the cone of light emanating from the fiber is coupled outside the receiving fibers and consequently the light intensity at the detector is reduced

For the experiments conducted in this work, a bifurcated bundle of optical fibers, with concentric traverse inside (CTI) grouping of the fibers at the merger point, was selected

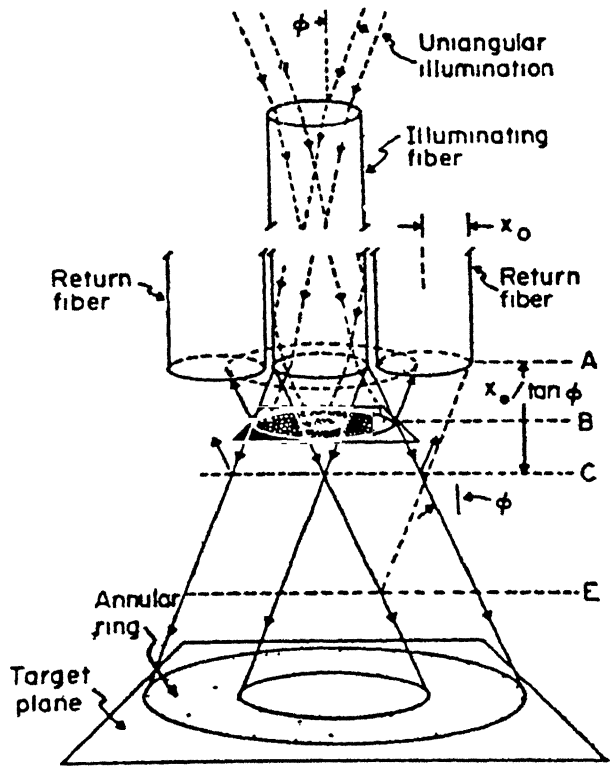


Fig 2 4 Operating principle of the optical fiber

## 2.3.2 Sensing And Amplification Circuit

Photodetection involves measuring the incident light in terms of an electrical signal There are three basic forms of photodetection They involve the photoemission, photoconduction and the photovoltaic actions Photoemission involves incident light that frees electrons from the detector surface This usually occurs in a vacuum tube With photoconduction the incident light on a photosensitive material causes the photodetector to alter its conductance In the photovoltaic action, a voltage is generated when the light strikes the sensitive material of photodetector

The most popular photodetector is the single junction photodiode A photodiode is the optical version of the standard diode It is constructed of a *P-N* junction Photons of light energy are absorbed into the device and the Hole-Electron pairs are generated The pairs are combined at different depths within the diode depending upon the energy level of the photon A wide, thin surface area is used to ensure the maximum absorption Current flow is dependent on the amount of radiation absorbed Photodiodes operate in the photoconductive mode with reverse DC bias applied This is also called as the current mode Current is extracted as a measure of the applied radiant energy Signal current flows through the load resistor, $R_1$, in the photoconductive circuit, as shown in Figure 2 5

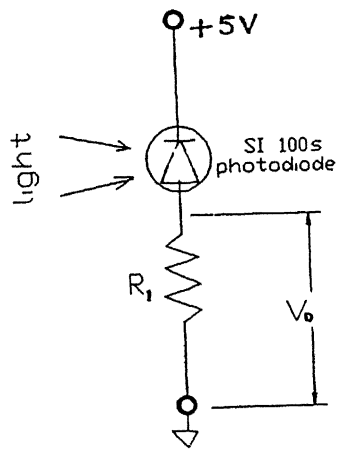


Fig 2 5 Photodiode circuit

A detector material is specially selected so that when it is exposed to light rays it will absorb the light energy If the detector responds to the light energy and not the wavelength, it is said to be non selective Selectivity or responsivity is the detector's response per unit of light Wavelength responsivity is called the spectral response Frequency response is the speed by which the detector responds to the changes in the radiation amplitude fluctuation in the output current and /or voltage, referred to as noise Noise is usually caused by current, which flows in the detector, regardless of whether light is applied A common specification for the detector is the signal-to-noise ratio, which is a ratio of the signal current and the noise current

In the present work, a *SI* 100s photodiode with the responsivity of 0 4 A/W at 632 8nm wavelength is used The specifications are shown in the Appendix A 10mW continuous He-Ne Laser gun is used as the light source

As the output voltage available after the photodiode is in terms of only a few millivolts, a pre-amplification circuit is required before using the signals. A two stage pre-amplification circuit has been designed and fabricated using a special purpose operational amplifier OP-07 The circuit is shown in the Figure 2 6

An operational amplifier amplifies the difference between the voltage signals at the two inputs, and can operate either in inverting or non-inverting mode The voltage developed across the load resistor of the photodiode, $R_1$, is fed as one input to the op-amp, the other input is grounded with the other resistor, $R_2$; $R_3$ being the feedback resistor Required factor of gain is obtained by using the appropriate values of the two resistors, $R_3$ and $R_2$ Initially with the two inputs of the op-amp

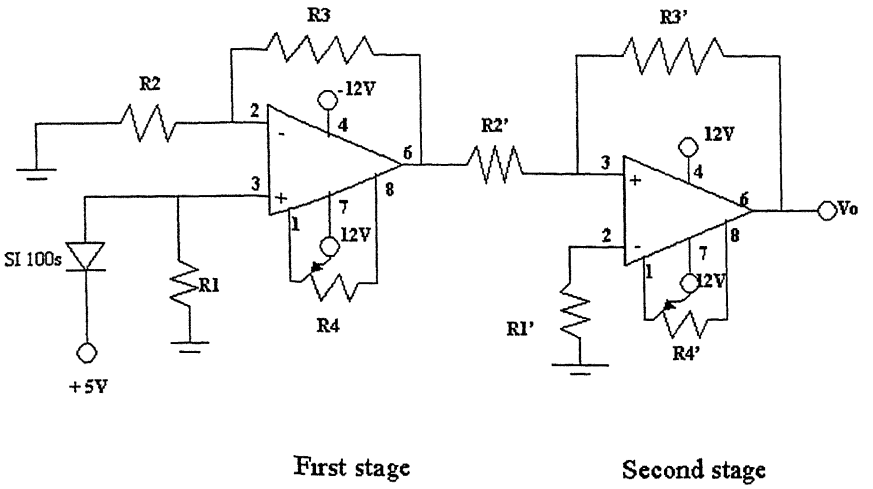


Figure 2 6 The sensing and amplification circuit (two stages)

shorted and grounded, the output voltage is set to zero using the variable resistor $R_4$ this is called the input offset voltage correction This is to be done carefully before using the circuit otherwise the op-amp will be driven into a saturation region giving a constant output voltage for any input signal The gain used in every stage of the circuit in the present work is calculated as follows.

(Gain at every stage) $G = 1 + \frac{R_3}{R_2}$

$$V_o = G(V_3 - V_2)$$

$$= (1 + \frac{R_3}{R_2})(I_p R_1)$$

$$= (1 + \frac{R_3}{R_2})\rho P R_1$$

## 2.4 Thermo-Electric Thermometry [30]

### 2.4.1 Thermocouple

If the two wires of different materials A and B are connected in the circuit as show in the Figure· 2 7, with one junction at the temperature $T_1$ and other at temperature $T_2$, an emf is generated, and if an ammeter is connected, a current flows in the circuit The magnitude of the emf generated in the circuit depends upon the temperature difference of the junctions $T_1$ and $T_2$ and the materials of A and B. The overall relationship between the voltage $E_s$ and temperatures $T_1$ and $T_2$ under zero current conditions, which is the basis of thermo-electric thermometry, is called *Seebeck effect*

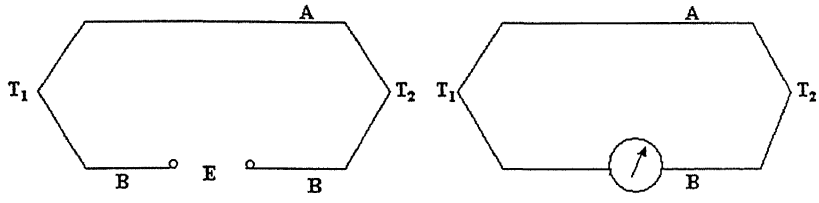


Fig 2 7 Thermocouple Circuit [30]

The emf developed in a thermo-electric circuit is ascribed to two phenomena, one is known as *Peltier effect* and other as *Thomson effect* Peltier effect concerns the reversible evolution, or absorption of heat that usually takes place when an electric current crosses a junction between two dissimilar metals This effect takes place whether the current is introduced externally or induced by the thermocouple itself External heating, or cooling, of the junction results in the reversal of the Peltier

effect, i e , a net electric current will be induced in one direction Thomson effect concerns the reversible evolution, or absorption of heat, occurring whenever an electric current traverses a single homogeneous conductor, across which a thermal gradient is maintained regardless of external introduction of current or its induction by the thermocouple itself The magnitude and the direction of the Thomson voltage setup in a single conductor depend upon temperature level, temperature difference, and the material The Thomson voltage alone cannot sustain a current in a single homogeneous conductor forming a closed circuit, since equal and opposite emfs will be set up in the two paths from heated to cooled parts The emf generated due to the Thomson effect is less predominant than that from the Peltier effect

The total emf acting in the circuit is the results of four emf's, two due to Peltier effect (one at each junction) and two due to Thomson effect The Peltier emf's are assumed proportional to the temperature difference of the junctions, while the Thomson emf's are proportional to the difference between the squares of the junction temperatures For the total emf $E_S$ the equation takes form

$$E_S = C_1 ( T_1 - T_2 ) + C_2 ( T_1^2 - T_2^2 )$$

For Cu-constantan couple,

$$C_1 = 37\ 5\ \mu V/\ K$$

$$C_2 = -0\ 045\ \mu V/(\ K)^2$$

The polarity of the emf depends upon the particular metal used and by the relationship of the temperatures at the two junctions

Materials of the thermocouple are selected such that the Thomson effect can be disregarded and the total emf is the sum of Peltier emf's only and thus depends only on the difference of the junction temperatures If the temperature at one junction (reference junction) is kept constant, emf generated is used to measure the temperature change

## 2.4.2 Laws of thermocouple

The following laws are very useful as they govern both theory and the practice of thermocouples

(i) Law of homogeneous circuit

*The thermo-electric current cannot be sustained in a circuit of a single homogeneous material, however varying in cross-section, by the application of heat alone*

The consequence of this law is that two different materials are required for any thermocouple circuit

(ii) Law of intermediate materials

*Insertion of an intermediate metal into a thermocouple circuit will not affect a net emf provided the two junctions introduce by the third material are at identical temperature*

This law suggests that a device for measuring thermo-electric emf, may be introduced into circuit at any point without affecting the net emf, provided all the junctions which are added to the circuit by introducing the device are all at the same temperature The proof of this statement is given in the Figure 2 8a

(iii) Law of intermediate temperature

*If a single thermocouple develops a net emf, E, when its junctions are at temperatures $T_1$ and $T_2$, and an emf, E , when itf junctions are at $T_2$ and $T_3$, it will develop an emf $E_1 = E + E$ , when its junctions are at temperatures $T_1$ and $T_3$*

The proof of this statement is given in Figure 2 8b A consequence of this law permits a thermocouple calibrated for a given temperature to be used with any other reference temperature through the use of a suitable correction Also the extension wires having the same thermo-electric characteristics as those of the

thermocouple wires can be introduced in the circuit without affecting the net emf of thermocouple

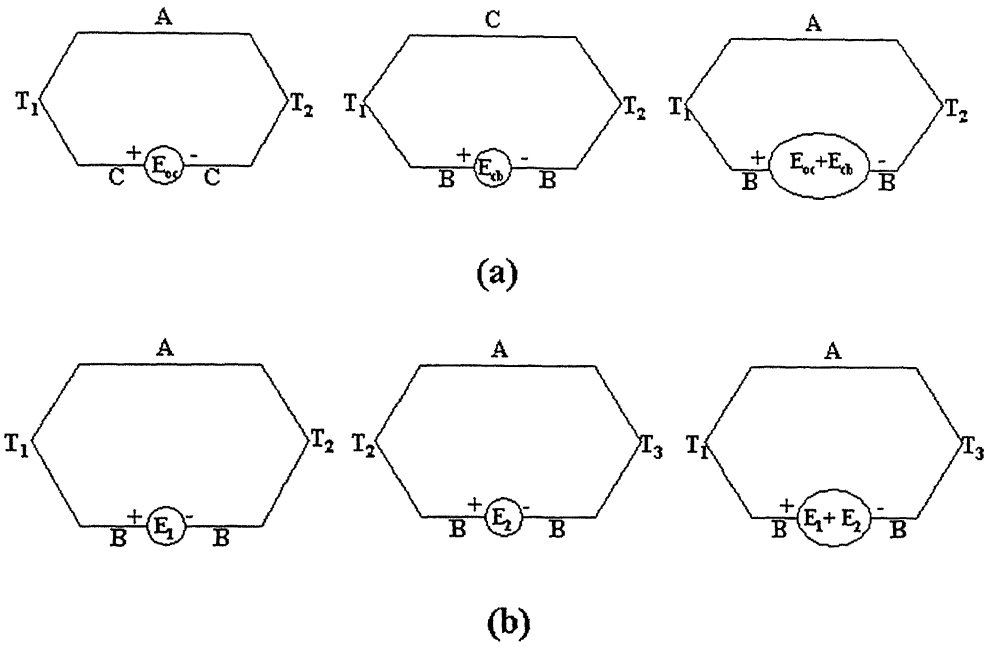


Fig 2 8 Thermocouple laws [30]

# *Chapter-3*

## Experimental setup and Procedure

## 3.1 Stages in experiments

A number of experiments were carried out in order to calibrate the thermocouple and the optical sensor and then to use it for tool wear measurements The stages of experimentations are as given below

1- Experimentation to calibrate the fiber optic device for surface roughness measurement
2- To calibrate the thermocouple (tool and work-piece combination) for the machining zone temperature
3- Experimentations to obtain tool wear, machining zone temperature, surface roughness (Ra) values and from the fiber optic sensor signals, for different combinations of machining parameter using Design of Experiments
4- Some experiments were carried out for the validation of the results from DOE and Neural Network analysis

## 3.2 Experimental setup

In the present work, the amount of flank wear on a turning tool is indirectly determined without interrupting the machining operation, by monitoring the cutting zone temperature and the surface finish using the thermocouple made- up naturally due to the different tool and work-piece materials and the photo-electronic sensor respectively This sensor consists of a bifurcated optical fiber, a laser gun as the light source, a photo diode as a detector along with an amplification circuit A schematic diagram of the experimental setup is shown in the Fig. 3 1. Photographs in Fig 3 2 and Fig 3 3 show the experimental setup in two different views The Y shaped optical fiber is held on the side diametrically opposite to the cutting tool The optical fiber is fixed in such a way that it tip by a certain distance and its axis intersects lags the cutting the axis of rotation of the

work-piece This is to ensure that the laser beam is incident on and reflected back by the freshly produced work surface The optical fiber used has a core of 3mm diameter and the cladding of 5mm diameter. The core and the cladding are coupled with the brass sleeves at the ends

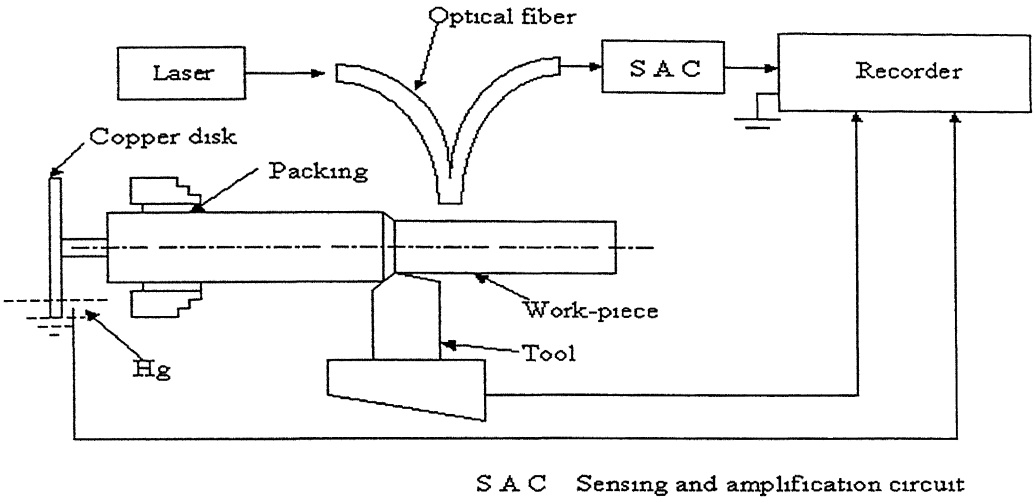


Fig 3 1 Schematic diagram of the experimental setup

A 10 mW continuous He-Ne laser gun is used as the light source He-Ne laser guns have the advantage of being handy over the solid state lasers The model (105-1) of *Uniphase Inc* is used The power of the laser beam should be such that it does not drive the photodiode into the saturation region and yet provide the signals of sufficient strength It is necessary to ensure that the laser beam produced is of a constant intensity throughout the experiments A brass coupling as shown in the Fig 3 4 is used to connect the source fibers of the sensors to the laser gun This is to ensure that there is no relative motion between the source fibers and the laser gun

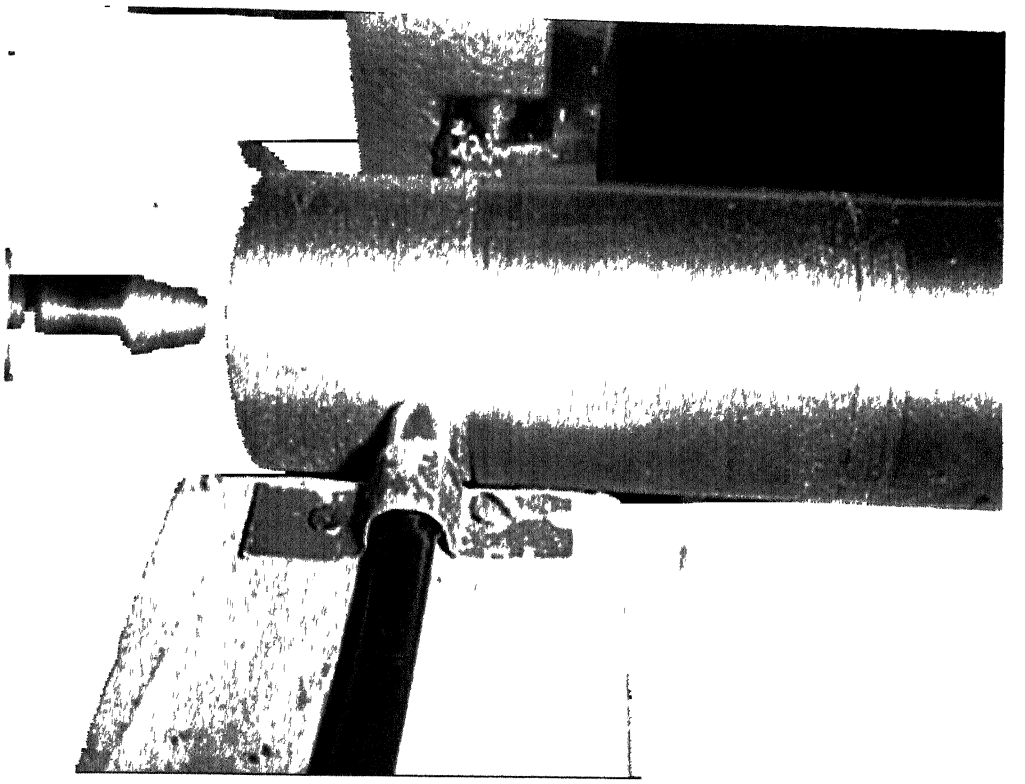

Figure 3 2 Photograph of the setup

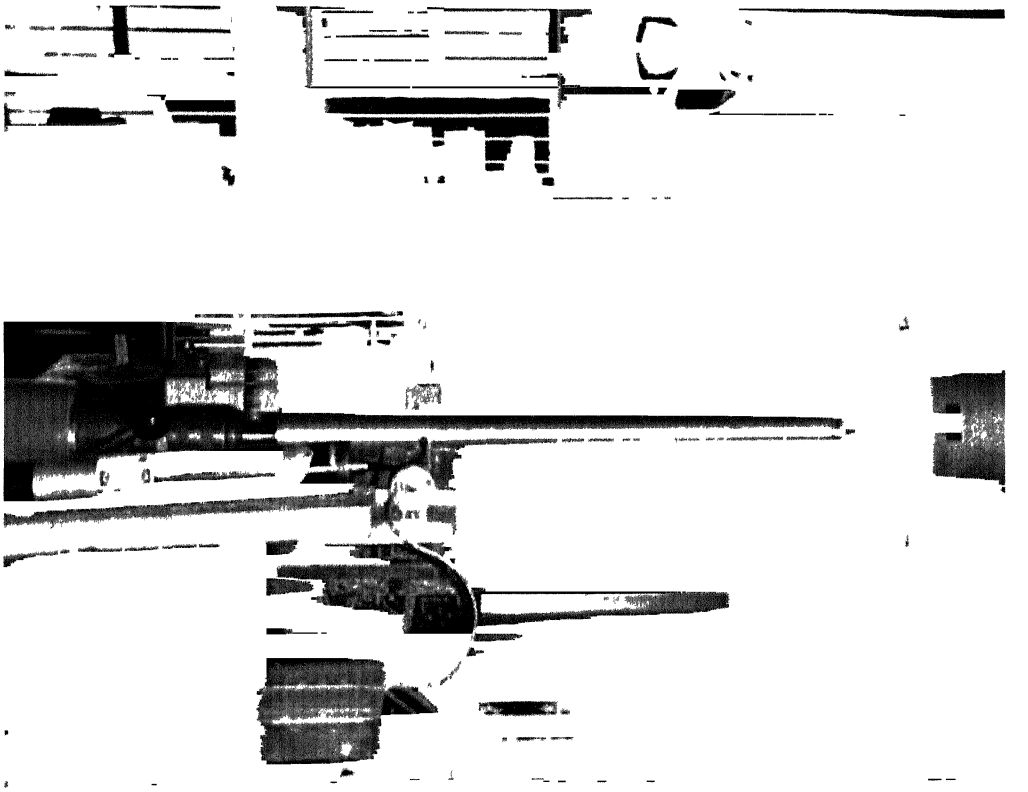

Figure 3 3 Full view of the setup

The sensing fibers were connected to the photodiode using another brass coupling(II), as shown in Fig 3 5, to ensure that the light coming to the photodiode is the light from the laser gun only and this coupling is also necessary to avoid any relative movement between the sensing fibers and the photodiode This setup ensures that any change in the output signal is only because of the change in the intensity of the reflected light

The output signal from the photodiode is connected to the amplification circuit Before using the amplification circuit the input voltage offset should be corrected using the variable resistor ($R_4$) in the circuit The circuit should give a zero output when the two inputs to the operational amplifier are short circuited and grounded Shielded cables with BNC connectors are used in the circuit to avoid noise in the output signal The photodiode and the operational amplifier are powered using a regulated DC power supply system The amplified signal is then fed to the recorder The amplifier is powered by a DC power supply of +5 V and +/-12 V

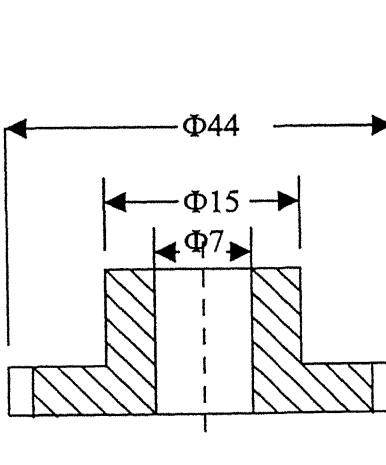


Figure 3 4 Brass coupling (I)
(All dimensions are in mm )

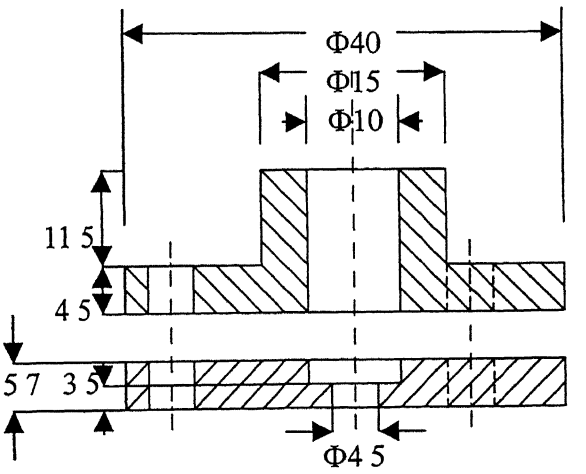


Figure 3 5 Brass coupling (II)
(All dimensions are in mm)

The signals from the naturally formed thermocouple (between tool and work-piece) are obtained by using a special arrangement In this arrangement an iron rod is screwed to the work piece at one end of it, which is mounted on the four-jaw chuck On the other end of the rod a copper disk is mounted, which rotates along with the chuck This disk is dipped into the mercury bath, from where a wire is taken out to the recorder On the other

hand, a wire is soldered to the tool also, which connects the tool with the recorder When the tool and work-piece come into the contact, the circuit is complete The tool and work-piece junction acts as the hot junction while machining is on and the other ends of work-piece and the tool at room temperature, act as cold junction To avoid the noise in the thermocouple signals, whole work-piece and the tool were insulated from the rest of the machine

The cutting conditions (speed, feed and depth of cut) form the inputs to the Neural Network program, trained a priori The Neural Network program predicts the outputs in terms of flank wear, temperature and surface finish signals The same cutting conditions forms the inputs for the regression equations for the same output as those from the neural network program We obtain these regression equations through MINITAB, which is a software for the Design of Experiments (DOE)

For the experiments, EN-24 steel was used as the work-piece and the HSS with 10% Cobalt as the cutting tool. The material compositions and the tool geometry are given in the Appendix The tool geometry, the tool height and the tool overhang are maintained uniformly for all experiments Gauges were used to set the tool height and the tool overhang before starting each experiment The range of the cutting parameters to be used were found from the handbooks and the machine capabilities as

Cutting speed (V) 20 to 35 m/min

Feed (F) 0 075 to 0 125 mm/rev

Depth of cut (D) 0 4 to 0 8 mm

These are depicted in table 3 1

| Level | V(m/min ) | F(mm/rev) | D(mm) |
|---|---|---|---|
| -1 | 20 | 0 075 | 0 4 |
| 0 | 27 5 | 0 1 | 0 6 |
| 1 | 35 | 0 125 | 0 8 |

Table 3 1 Level designation of different process variables

For different input parameters, level can be calculated by the formula

level = (actual value – mean value of the range )/(maximum value - mean value of the working range of the parameter)

so, v = (V – 27 5)/ 7 5

Where 'v' is the level of cutting speed Similarly for feed and depth of cut, the levels can be calculated as

f = (F – 0 1)/ 0 025,

and, d = (D – 0 6)/ 0 2

Where 'f' and 'd' are levels of feed and depth of cut respectively

The different levels of the variables (cutting speed, feed and the depth of cut), which were used in different experiments, according to the $3^3$ factorial design of DOE, are given in the table 3 2. The levels of the process variables, which were used for the experiments of the validation set, were in between the [–1,1] range, where –1 stands for the minimum and +1 stands for the maximum level of parameters

The work-piece was held in a four-jaw chuck and supported by a revolving center at the tailstock A rough turning pass was taken to obtain the desired initial work-piece diameter. The other cutting parameters (feed and depth of cut) were set as required for the particular experiment After machining with a fresh tool for about 1cm length of work-piece, the process was stopped and the initial gap between the freshly generated surface of the work-piece and the bifurcated optical fiber was adjusted to the 2mm (initial experiments showed that the sensor signals varied linearly with the change in gap up-to 3 5mm and then starts decreasing on increasing the distance between them) Then the machining operations continued for the rest of the work-piece length During machining, the sensor output from the optical sensor system and the thermocouple were recorded, and the output signals at the end of machining were given to the Neural Network program as the inputs for the training along with the other cutting conditions (speed, feed and depth of cut)

| Experiment No | V level (v) | F level (f) | D level (d) |
|---|---|---|---|
| 1 | -1 | -1 | -1 |
| 2 | -1 | -1 | 0 |
| 3 | -1 | -1 | 1 |
| 4 | -1 | 0 | -1 |
| 5 | -1 | 0 | 0 |
| 6 | -1 | 0 | 1 |
| 7 | -1 | 1 | -1 |
| 8 | -1 | 1 | 0 |
| 9 | -1 | 1 | 1 |
| 10 | 0 | -1 | -1 |
| 11 | 0 | -1 | 0 |
| 12 | 0 | -1 | 1 |
| 13 | 0 | 0 | -1 |
| 14 | 0 | 0 | 0 |
| 15 | 0 | 0 | 1 |
| 16 | 0 | 1 | -1 |
| 17 | 0 | 1 | 0 |
| 18 | 0 | 1 | 1 |
| 19 | 1 | -1 | -1 |
| 20 | 1 | -1 | 0 |
| 21 | 1 | -1 | 1 |
| 22 | 1 | 0 | -1 |
| 23 | 1 | 0 | 0 |
| 24 | 1 | 0 | 1 |
| 25 | 1 | 1 | -1 |
| 26 | 1 | 1 | 0 |
| 27 | 1 | 1 | 1 |

Table 3 2. Levels of the process variables in different experiments

In most of the experiments, an initial increase in the voltage signals from the optical sensor system was observed as against the expected decrease in the same It is known that the amount of light reflected from the work-piece surface and detected at the photodiode end, depends only on the distance between the sensor and the work piece surface and the surface roughness or the reflectance of the surface of work-piece Some time after the machining operation is started with a fresh tool, the sharp cutting tip on the tool gets blunted and a small nose radius is formed This results in better surface finish of the work-piece and hence higher reflectance Further drop in the voltage signals during the

machining operation is due to the slightly bad surface quality produced by the tool, due to the wear, than it was at the start of cutting

## 3.3 Calibration of the Optical Sensing System

A graph was plotted for calibrating the signals from the Optical sensing system with the experimental roughness value obtained by the Telesurf (surface roughness measuring instrument) A total number of eighteen calibrating points (Table 3 3) are used to plot the graph The equation of the best fit line is given by

$$Ra = 10\,91 - 5\,99 \times (s\,f \text{ in volts})$$

| S\n | s f (in volts) | Ra (μ) |
|---|---|---|
| 1 | 0 730 | 6 39 |
| 2 | 0 443 | 6 94 |
| 3 | 0 464 | 6 69 |
| 4 | 0 598 | 8 00 |
| 5 | 0 395 | 8 35 |
| 6 | 0.456 | 9 58 |
| 7 | 0.497 | 9.22 |
| 8 | 0 487 | 9 71 |
| 9 | 0 550 | 7.78 |
| 10 | 0 391 | 7.13 |
| 11 | 0 477 | 8.12 |
| 12 | 0 583 | 8.52 |
| 13 | 0 893 | 5.42 |
| 14 | 0 450 | 6.78 |
| 15 | 0 710 | 5.57 |
| 16 | 0 550 | 6.46 |
| 17 | 0 440 | 8.60 |
| 18 | 0 463 | 9.72 |

Table 3 3 Calibrating points for the calibration of optical sensing system

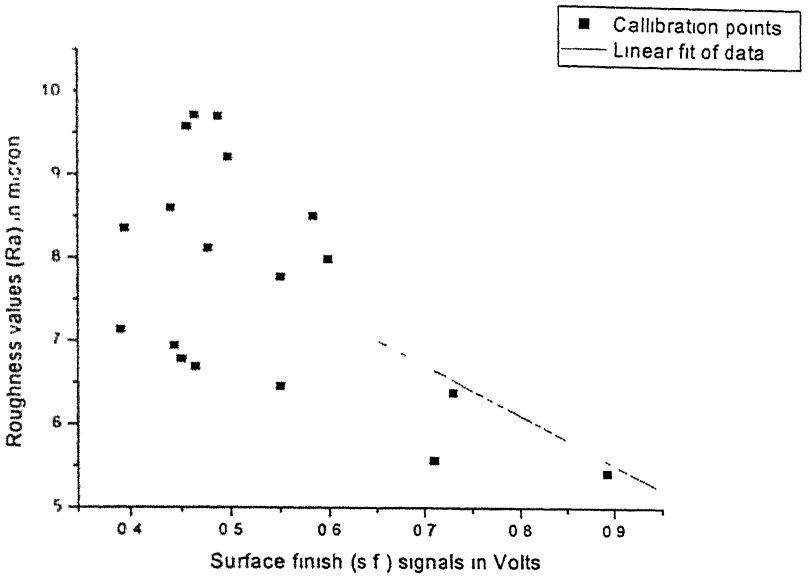


Figure 3 6 Calibration of signals from Optical Sensor system with Roughness values

## 3.4 Calibration of the Thermocouple

For the calibration of the thermocouple made by the tool and work-piece materials' combination, a junction of the bits of the above two materials was made and put in the lead bath This junction works as hot junction, the ambient air temperature works as cold junction temperature, when lead bath (i e the hot junction) is heated up, a small emf is generated which is recorded on a recorder (Seebek effect) Temperature of the lead bath is measured by using a digital temperature indicator.

A graph between signals from thermocouple and the relative temperatures, obtained from the calibration experiments (Table 3 4) is shown in figure 3 7

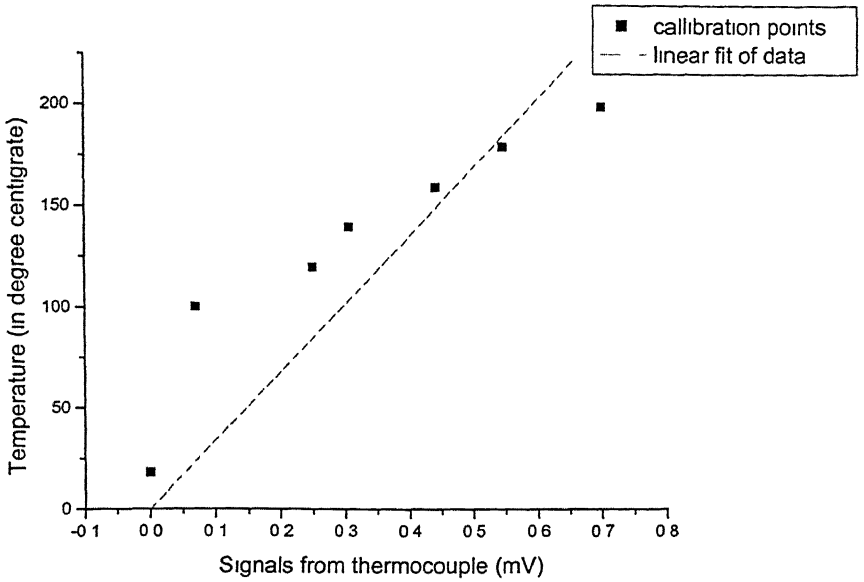


Figure 3 7 Calibration of the signals from Thermocouple with Temperature

A total number of seven calibrating points (Table 3 4) are used to plot the graph The equation of the best-fit line is given by

Temp(°C) = 340 21296 x (signals from the thermocouple in mV)

| S\n | Signals from thermocouple (mV) | Temperature (°C) |
|---|---|---|
| 1 | 0 | 18 |
| 2 | 0 07 | 100 |
| 3 | 0 25 | 120 |
| 4 | 0 305 | 140 |
| 5 | 0 44 | 160 |
| 6 | 0 545 | 180 |
| 7 | 0 7 | 200 |

Table3 4 Calibration points for the calibration of the Thermocouple

# *Chapter 4*

## Results and Discussions

### 4.1 Results obtained from the training set of experiments

Design of experiments is normally used to reduce the total number of experiments required for studying the behaviour of any system However it is known that a Neural Network (NN) program learns better with a large number of training data Keeping this in view, a total number of thirty-two experiments were performed after the initial set of trial experiments

The cutting conditions used and the output parameters (e g the flank wear on the cutting tool, surface roughness of the generated surface, voltage signals from the optical sensor system and the temperature) obtained from the experiments (along with DOE and NN analysis results) are shown in the table 4 1, and table 4 2

Twenty seven of the thirty-two experiments were used {as given by $3^3$ model of Design of Experiments (DOE)} for the training and rest of them (five) were used as the validation set, to validate the results from the DOE and the Neural Network (NN) models Network was trained separately for each output

As there is no standard criterion for selecting the neurons in the hidden layer of the network, the learning rate constants and the momentum constant, networks with different topological characteristics were tried The learning behaviours of these networks were studied and the one with an architecture of 3-7-1 was selected for predicting different outputs (e g the flank wear on the cutting tool, surface roughness of the generated surface, voltage signals from the optical sensor system and the temperature) The learning behaviour of this particular network is shown in Figure 4 1. Training of the Neural

Network was done with an allowable error of 0 01 (sum of squared error over the output neurons) and took about 120 minutes

Once the network is trained such that the maximum error for any of the training data is less than the allowable error, the weights and the threshold values are automatically saved by the program As the input values from the validation experiments are given to the NN program, the program predicts the required output

The analysis using the Design of experiments was made by using a DOE software called 'MINITAB' The software took the cutting conditions and responses from the experiments, which were used for training the Neural Network and develops the regression equations for each desired output The machining conditions from the validation set were given to the regression equations as the inputs and the equations, in turn provided the predictions for the different outputs (e g the flank wear on the cutting tool, surface roughness of the generated surface, voltage signals from the optical sensor system and the temperature)

The results from the DOE analysis and the NN program were then compared to get a view that which one of the analysis gives the results, nearer to the experimental values.

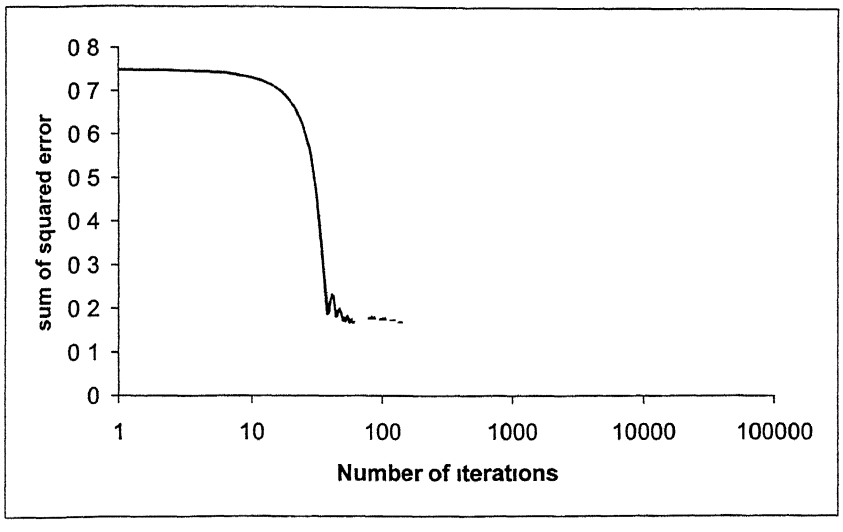


Figure 4 1 Learning behaviour of the Neural Network

| S\n | v | f | d | s f (V) (DOE) | s f (V) (NN) | s f (V) (Exp ) | Ra (μ) Calli (DOE) | Ra (μ) Calli (NN) | Ra (μ) Calli (Exp ) |
|---|---|---|---|---|---|---|---|---|---|
| 1 | -1 | -1 | -1 | 0 567 | 0 662 | 0 73 | 7 51 | 6 94 | 6 54 |
| 2 | -1 | -1 | 0 | 0 495 | 0 51 | 0 443 | 7 95 | 7 86 | 8 26 |
| 3 | -1 | -1 | 1 | 0 410 | 0 398 | 0 38 | 8 46 | 8 53 | 8 63 |
| 4 | 0 | -1 | -1 | 0 499 | 0 531 | 0 464 | 7 92 | 7 73 | 8 13 |
| 5 | 0 | -1 | 0 | 0 460 | 0 532 | 0 598 | 8 16 | 7 72 | 7 33 |
| 6 | 0 | -1 | 1 | 0 407 | 0 331 | 0 395 | 8 47 | 8 93 | 8 54 |
| 7 | 1 | -1 | -1 | 0 547 | 0 4 | 0 456 | 7 63 | 8 51 | 8 18 |
| 8 | 1 | -1 | 0 | 0 541 | 0 561 | 0 497 | 7 67 | 7 55 | 7 93 |
| 9 | 1 | -1 | 1 | 0 521 | 0 554 | 0 487 | 7 79 | 7 59 | 7 99 |
| 10 | -1 | 0 | -1 | 0 534 | 0 419 | 0 351 | 7 68 | 8 40 | 8 81 |
| 11 | -1 | 0 | 0 | 0 499 | 0 429 | 0 362 | 7 92 | 8 34 | 8 74 |
| 12 | -1 | 0 | 1 | 0 446 | 0 483 | 0 55 | 8 24 | 8 02 | 7 62 |
| 13 | 0 | 0 | -1 | 0 475 | 0 435 | 0 391 | 8 06 | 8 30 | 8 57 |
| 14 | 0 | 0 | 0 | 0 468 | 0 463 | 0 477 | 8 11 | 8 14 | 8 05 |
| 15 | 0 | 0 | 1 | 0 448 | 0 479 | 0 468 | 8 23 | 8 04 | 8 11 |
| 16 | 1 | 0 | -1 | 0 528 | 0 516 | 0 583 | 7 75 | 7 82 | 7 42 |
| 17 | 1 | 0 | 0 | 0 553 | 0 837 | 0 893 | 7 60 | 5 90 | 5 56 |
| 18 | 1 | 0 | 1 | 0 566 | 0 516 | 0 45 | 7 52 | 7 82 | 8 21 |
| 19 | -1 | 1 | -1 | 0 508 | 0 642 | 0 71 | 7 86 | 7 06 | 6 66 |
| 20 | -1 | 1 | 0 | 0 500 | 0 388 | 0 37 | 7 92 | 8 59 | 8 69 |
| 21 | -1 | 1 | 1 | 0 478 | 0 482 | 0 55 | 8 05 | 8 02 | 7 62 |
| 22 | 0 | 1 | -1 | 0 449 | 0 406 | 0 473 | 8 22 | 8 48 | 8 08 |
| 23 | 0 | 1 | 0 | 0 473 | 0 473 | 0 46 | 8 08 | 8 08 | 8 15 |
| 24 | 0 | 1 | 1 | 0 484 | 0 507 | 0 44 | 8 01 | 7 87 | 8 27 |
| 25 | 1 | 1 | -1 | 0 505 | 0 508 | 0 463 | 7 88 | 7 87 | 8 14 |
| 26 | 1 | 1 | 0 | 0 562 | 0 521 | 0 454 | 7 54 | 7 79 | 8 19 |
| 27 | 1 | 1 | 1 | 0 606 | 0 583 | 0 65 | 7 28 | 7 42 | 7 02 |

Table 4 1 Comparison of Experimental values with the predicted values of Surface finish signals and the Roughness values (from calibration) for the training set of experiments

| S\n | v | f | d | Temp °C (DOE) | Temp °C (NN) | Temp °C (Exp ) | Wear (mm) (DOE) | Wear (mm) (NN) | Wear (mm) (Exp ) |
|---|---|---|---|---|---|---|---|---|---|
| 1 | -1 | -1 | -1 | 483 7 | 487 23 | 452 14 | 0 356 | 0 322 | 0 254 |
| 2 | -1 | -1 | 0 | 518 9 | 524 52 | 520 53 | 0 464 | 0 502 | 0 57 |
| 3 | -1 | -1 | 1 | 536 3 | 567 82 | 527 33 | 0 355 | 0 386 | 0 32 |
| 4 | -1 | 0 | -1 | 506 7 | 547 1 | 544 34 | 0 345 | 0 373 | 0 44 |
| 5 | -1 | 0 | 0 | 552 1 | 577 96 | 618 51 | 0 473 | 0 512 | 0 577 |
| 6 | -1 | 0 | 1 | 579 7 | 603 66 | 611 36 | 0 384 | 0 399 | 0 381 |
| 7 | -1 | 1 | -1 | 587 5 | 557 72 | 580 06 | 0 211 | 0 245 | 0 22 |
| 8 | -1 | 1 | 0 | 643 1 | 577 4 | 613 74 | 0 360 | 0 29 | 0 222 |
| 9 | -1 | 1 | 1 | 680 9 | 595 51 | 618 51 | 0 290 | 0 321 | 0 254 |
| 10 | 0 | -1 | -1 | 586 3 | 556 5 | 554 55 | 0 496 | 0 448 | 0 381 |
| 11 | 0 | -1 | 0 | 620 9 | 573 24 | 613 74 | 0 618 | 0 567 | 0 508 |
| 12 | 0 | -1 | 1 | 637 7 | 594 46 | 632 80 | 0 522 | 0 505 | 0 572 |
| 13 | 0 | 0 | -1 | 577 2 | 576 51 | 563 05 | 0 508 | 0 503 | 0 57 |
| 14 | 0 | 0 | 0 | 622 | 627 94 | 603 54 | 0 65 | 0 629 | 0 667 |
| 15 | 0 | 0 | 1 | 649 | 676 63 | 646 40 | 0 574 | 0 544 | 0 572 |
| 16 | 0 | 1 | -1 | 625 9 | 686 84 | 646 40 | 0 398 | 0 431 | 0 413 |
| 17 | 0 | 1 | 0 | 680 9 | 717 58 | 677 02 | 0 560 | 0 614 | 0 572 |
| 18 | 0 | 1 | 1 | 718 1 | 737 73 | 777 73 | 0 504 | 0 639 | 0 572 |
| 19 | 1 | -1 | -1 | 634 7 | 665 27 | 673 62 | 0 536 | 0 631 | 0 699 |
| 20 | 1 | -1 | 0 | 668 7 | 664 96 | 690 63 | 0 672 | 0 674 | 0 73 |
| 21 | 1 | -1 | 1 | 684 9 | 663 67 | 704 24 | 0 590 | 0 639 | 0 572 |
| 22 | 1 | 0 | -1 | 593 5 | 586 47 | 572 58 | 0 571 | 0 547 | 0 48 |
| 23 | 1 | 0 | 0 | 637 7 | 600 38 | 640 96 | 0 727 | 0 639 | 0 572 |
| 24 | 1 | 0 | 1 | 664 1 | 618 87 | 578 36 | 0 665 | 0 587 | 0 635 |
| 25 | 1 | 1 | -1 | 610 1 | 619 21 | 615 79 | 0 484 | 0 513 | 0 446 |
| 26 | 1 | 1 | 0 | 664 5 | 667 81 | 627 35 | 0 66 | 0 694 | 0 762 |
| 27 | 1 | 1 | 1 | 701 1 | 711 9 | 752 55 | 0 618 | 0 686 | 0 622 |

Table 4 2 Comparison of experimental values with the predicted values of Temperature and Flank wear for the training set of experiments

The regression equations obtained from the DOE analysis based on experiments of training set, are as follows

Surface finish

$$s\,f(V) = 0\,468 + 0\,0067\,v + 0\,0271\,f - 0\,0139\,d - 0\,00178\,v^2 + 0\,0582\,f^2 - 0\,0065\,d^2 + 0\,0042\,v\,f + 0\,0330\,f\,d + 0\,0318\,v\,d$$

Temperature

$$\text{Temp } (^{\circ}C) = 622 + 42\,8\,v + 30\,f + 35\,9\,d - 27\,1\,v^2 + 28\,9\,d^2 - 8\,9\,f^2 - 32\,1\,v\,f + 10\,2\,f\,d - 0\,6\,v\,d$$

Flank wear ·

$$\text{Wear (mm)} = 0\,650 + 0\,127\,v - 0\,0291\,f + 0\,0332\,d - 0\,0499\,v^2 - 0\,0611\,f^2 - 0\,109\,d^2 + 0\,0231\,v\,f + 0\,0199\,f\,d + 0\,0136\,v\,d$$

Where v, f and d are levels of Cutting speed (V), Feed(F) and depth of cut (D) and values for these levels can be obtained by following formula

level = (actual value in the range – mean value of the range )/ increment for two subsequent levels

hence we get

$$v = (V - 27.5)/7\,5,$$

$$f = (F - 0\,1)/0\,025,$$

$$d = (D - 0\,6)/0\,02$$

By putting the levels of input parameters in the above equations one can predict the various output parameters But above equations give the best results only when the input levels are in between the ranges of input parameters taken to make a DOE analysis

### 4.1.1 Response surfaces for the regression equations

Response surface for the regression equation for the Surface finish signals is shown in the Figure 4 2 The figure clearly shows that the Surface finish signals increase with the increase of cutting speed This is according to the theory that the surface finish increases with the cutting speed But the results with the feed are entirely different as figure shows an initial decrease and then increase in the signals on increasing the feed, which is not in accordance with the theory

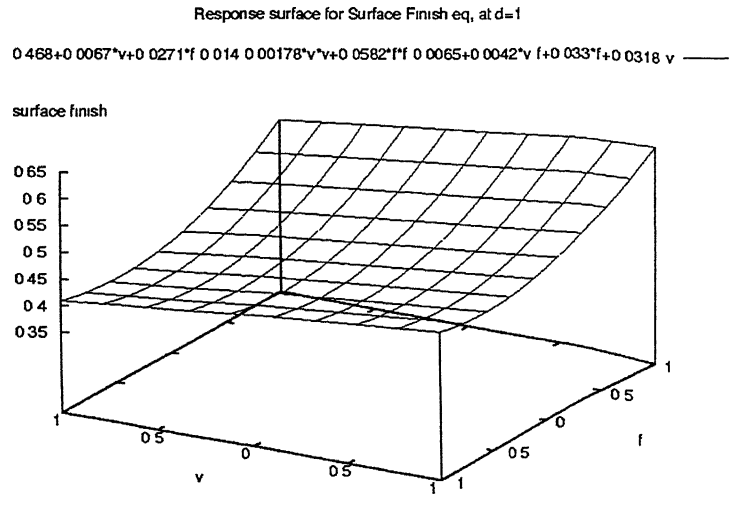


Figure 4 2 Response surface for the regression equation for the Surface finish signals (at d = 1)

Response surface for the regression equation for the Flank wear is shown in the figure 4 3 The figure clearly shows that the wear increases with the increase in cutting speed Also the wear increases with the increase in the feed, which is in accordance with the theory While the response surface for the regression equation for the Temperature of the cutting zone is shown in the Fig 4 4 The figure indicates that within a wide range the temperature increases with the increase in the cutting speed While in the whole range of feed the temperature increases with the increase in feed The figures 4 2 to figure 4 4

show the graphs for constant depth of cut at d = 1 level) The graphs obtained while keeping the cutting speed and feed constant (at maximum level) can be seen in the chapter 'Appendix' of the present work

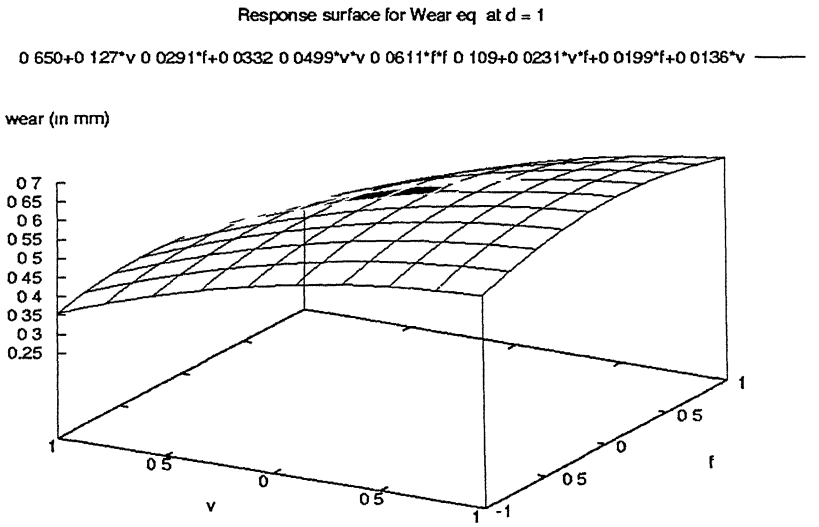


Figure 4 3 Response surface for the regression equation for the Flank wear (at d=1)

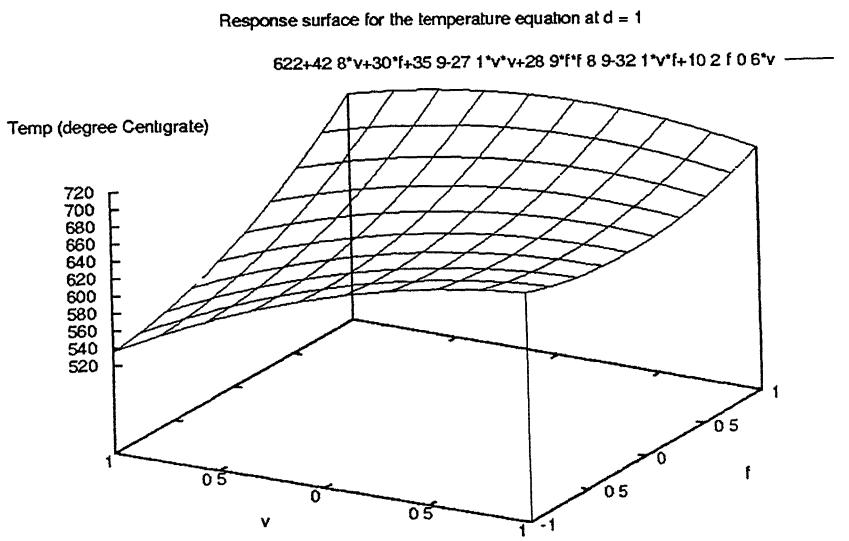


Figure 4 4 Response surface for the regression equation for the Temperature (at d=1)

### 4.1.2 Comparison of DOE predictions with experimental values of responses for the training set of experiments

Figure 4 5 shows the comparison between the wear predictions by Design of Experiment analysis and the experimental values over the range of cutting speed for different feed levels for the highest depth of cut level (d = 1)

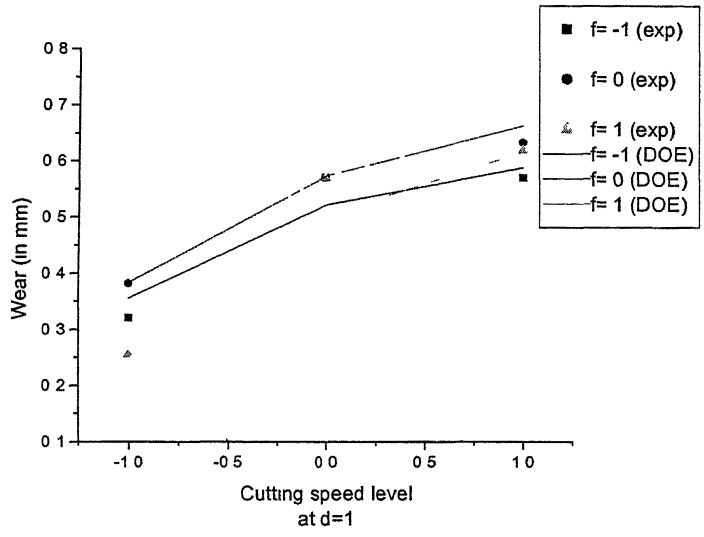


Fig 4 5 Comparison between DOE predictions and experimental values for wear at d = 1

Figure 4 6 shows the comparison between the predictions of surface finish signals obtained from DOE analysis and the experimental values over the whole range of cutting speed for different feeds while the level of depth of cut being at "1" While Figure 4 7 shows the same graph as figure 4 6 but in terms of the surface roughness values (Ra values) obtained from the calibration curve between the Surface finish signals and the Surface roughness values (Figure 3 6)

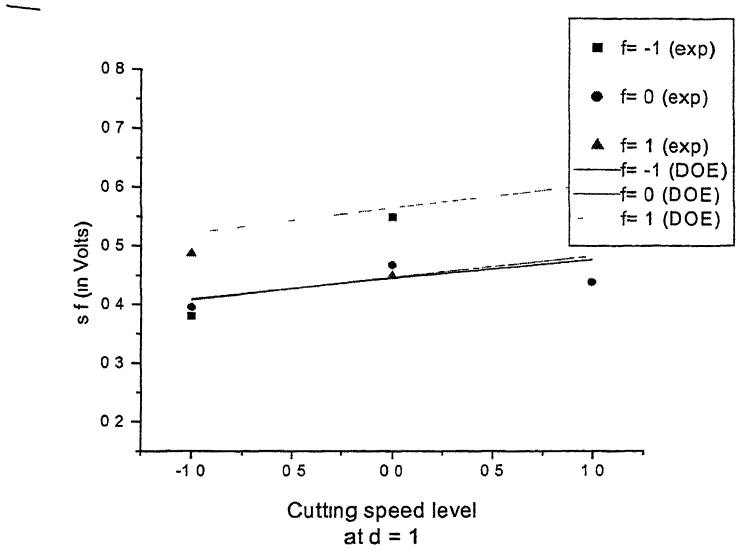


Fig 4 6 Comparison between DOE predictions and experimental values for Surface finish signals at d=1

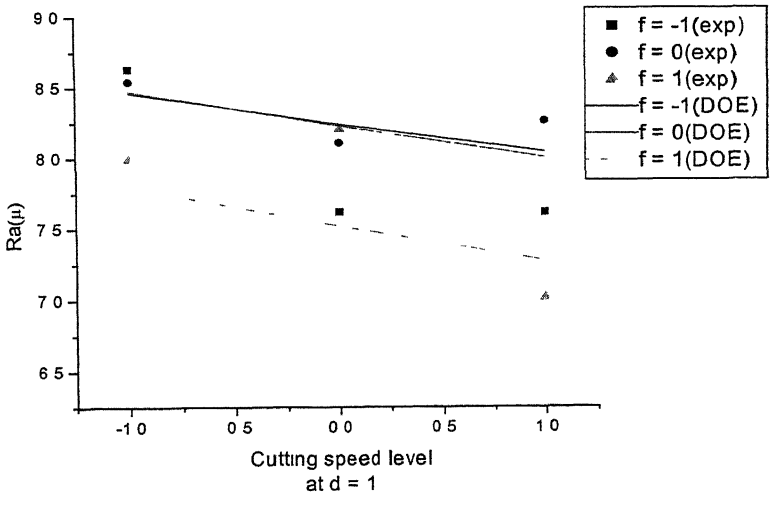


Fig 4 7 Comparison between DOE predictions and experimental values for the Surface roughness at d = 1

Figure 4 8 compares the DOE predictions for the cutting zone temperature and the experimental values over the whole range of cutting speed for each feed level at d =1

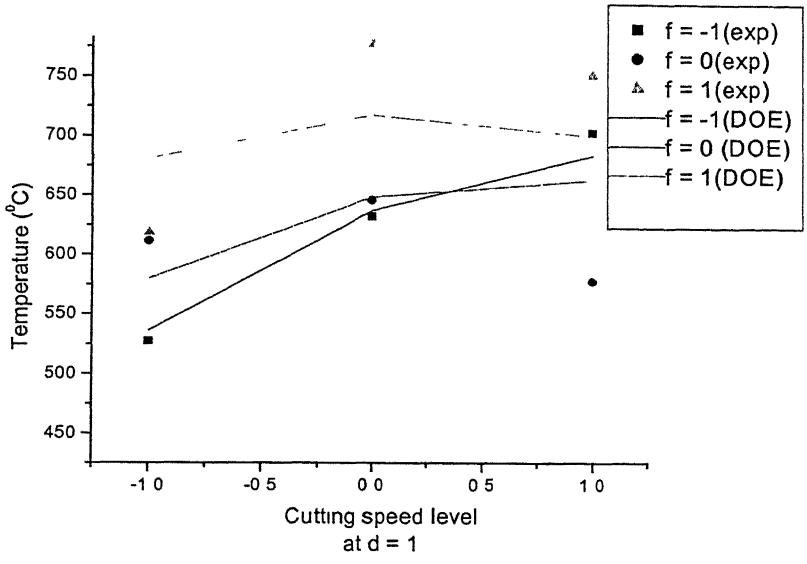


Fig 4 8 Comparison between DOE predictions and experimental values for cutting zone temperature at d = 1

Graphs in this section are for maximum depth of cut level (d = 1) Graphs for other depth of cut levels are shown in chapter 'Appendix'

### 4.1.3 Comparison of Neural Network predictions with Experimental values of responses for the training set of experiments

Figure 4 9 shows the comparison between the predictions by the Neural Network analysis and experimental values for wear over the whole range of cutting speed for each feed level at the maximum depth of cut level (d = 1) Figure 4 10 shows the Surface finish signal values from the neural network analysis and experiments being compared over the whole range of cutting speed for different levels of feed at d = 1

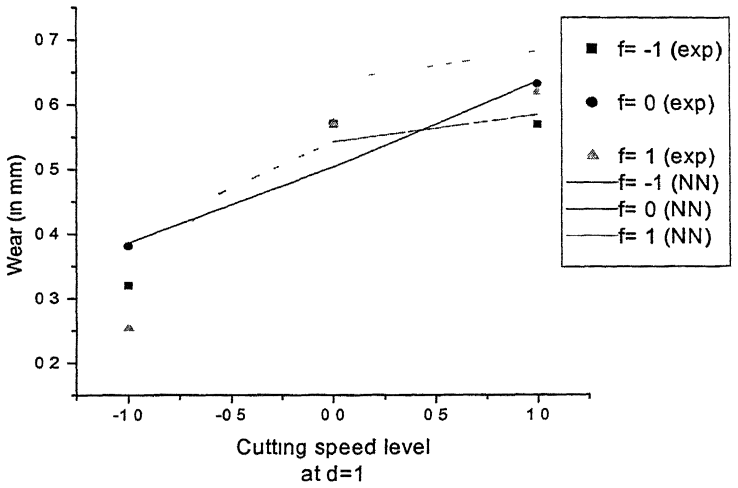


Fig 4 9 Comparison between NN predictions and experimental values for Wear at d = 1

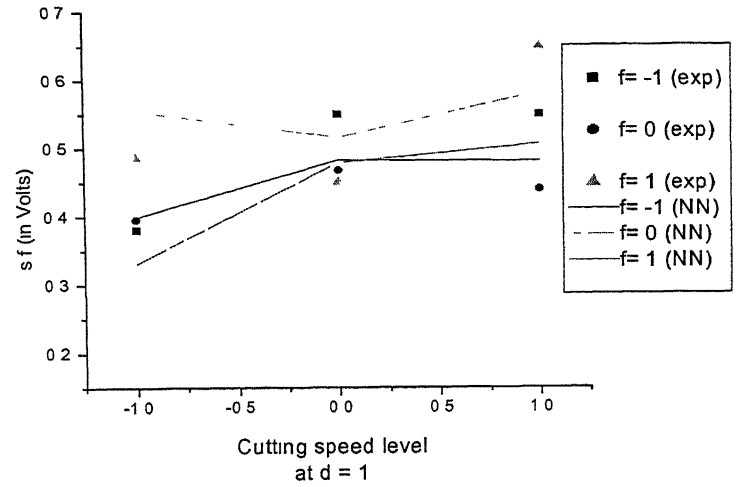


Fig 4 10 Comparison between NN predictions and experimental values for Surface finish signals at d = 1

Figure 4 11 depicts the same graph as in figure 4 10 but in terms of the roughness values obtained from the calibration curve between Surface finish signals and Roughness values

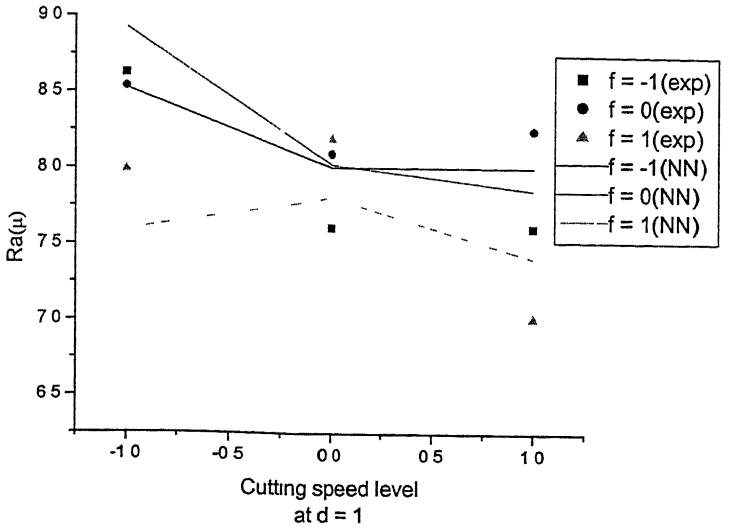


Fig 4 11 Comparison of NN predictions with experimental values for Surface roughness at d = 1

Figure 4 12 compares the values predicted by Neural Network and the experiments for the cutting zone temperature over the range of cutting speed for each feed level at level d = 1

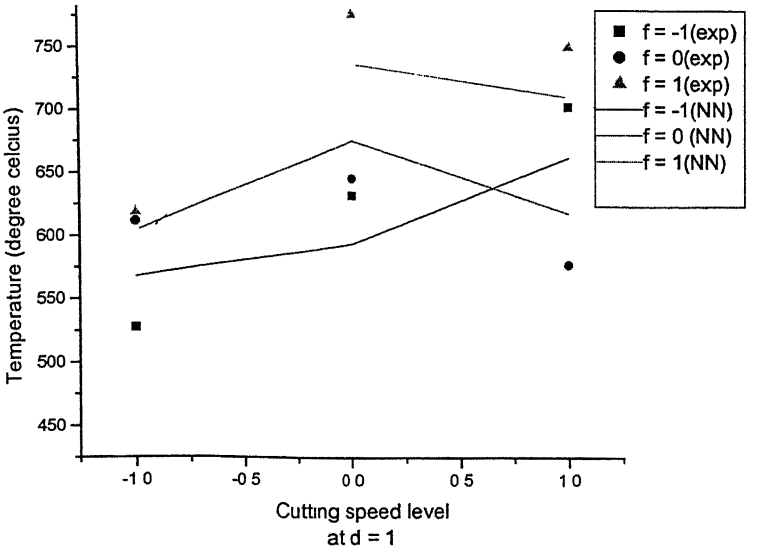


Fig 4 12 Comparison between NN predictions and experimental values for cutting zone temperature at d = 1

Above figures 4 9 to 4 12 shows the graphs pertaining to d = 1 level The graphs for other depth of cut levels are shown in chapter 'Appendix' of the present work

## 4.2 Results obtained from the validation set of experiments

As now we have ready to be used regression equations of all the response variables and also the trained Neural Network program, we can find out the predictions by both the techniques The predicted values of the responses, by both of the prediction methods (i e DOE and NN), are compared with the experimental values for the validation set of experiments Comparisons are given in the table 4 3 and table 4.4 for validation set of experiments respectively

| S\n | v | f | d | s f (V) (DOE) | s f (V) (NN) | s f (V) (Exp ) | Ra (μ) Calli (DOE) | Ra (μ) Calli (NN) | Ra (μ) Calli (Exp ) |
|---|---|---|---|---|---|---|---|---|---|
| 1 | -0 449 | -0 48 | 0 5 | 0 442 | 0 407 | 0 476 | 8 26 | 8 47 | 8 06 |
| 2 | 0 271 | -0 48 | -0 5 | 0 478 | 0 446 | 0 413 | 8 04 | 8 24 | 8 44 |
| 3 | 0 219 | 0 52 | -0 75 | 0 488 | 0 546 | 0 508 | 7 98 | 7 64 | 7 87 |
| 4 | 0 461 | 1 | 0 75 | 0 58 | 0 595 | 0 603 | 7 44 | 7 35 | 7 30 |
| 5 | -0 52 | 0 52 | 1 | 0 473 | 0 435 | 0 455 | 8 08 | 8 30 | 8 18 |

Table 4 3 Comparison of Experimental values with the predicted values of Surface finish signals and the Roughness values (from calibration) for the validation set of experiments

| S\n | v | f | d | Temp °C (DOE) | Temp °C (NN) | Temp °C (Exp ) | Wear (mm) (DOE) | Wear (mm) (NN) | Wear (mm) (Exp ) |
|---|---|---|---|---|---|---|---|---|---|
| 1 | -0 449 | -0 48 | 0 5 | 596 07 | 607 99 | 552 51 | 0 569 | 0 545 | 0 522 |
| 2 | 0 271 | -0 48 | -0 5 | 610 40 | 573 42 | 640 62 | 0 637 | 0 619 | 0 607 |
| 3 | 0 219 | 0 52 | -0 75 | 614 02 | 641 52 | 557 95 | 0 550 | 0 551 | 0 49 |
| 4 | 0 461 | 1 | 0 75 | 709 43 | 739 58 | 767 52 | 0 602 | 0 625 | 0 572 |
| 5 | -0 52 | 0 52 | 1 | 657 13 | 683 95 | 707 64 | 0 460 | 0 448 | 0 447 |

Table 4 4 Comparison of experimental values with the predicted values of Temperature and Flank wear for the validation set of experiments

### 4.2.1 Comparison between predicted values obtained by DOE and NN analyses and experimental values of responses for the validation set of experiments

Figure 4 13 compares the predicted values of the flank wear (by both the DOE and NN techniques) with the experimental ones, to show the variations from the experimental values

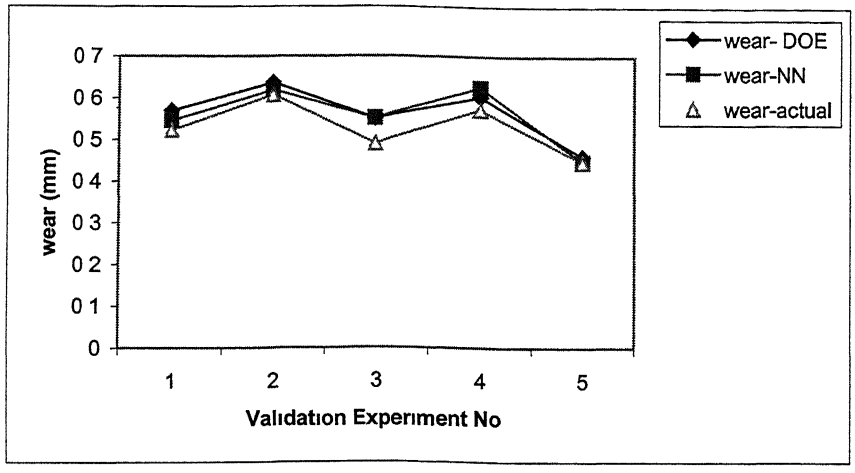


Fig 4 13 Comparison between predicted and experimental values of 'Flank wear'

Comparison of the predicted values of the surface finish signals by both the Design of Experiment and Neural Network techniques is shown in figure 4 14

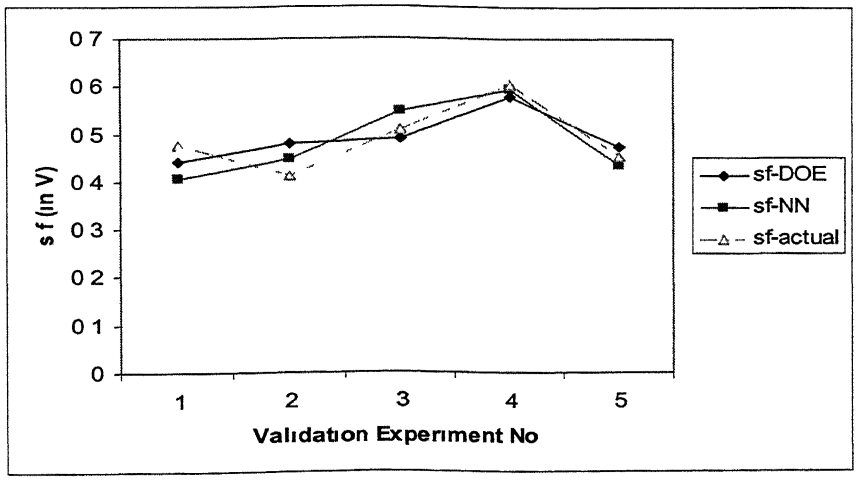


Fig 4 14 Comparison between predicted and experimental values of 'Surface finish signals'

Comparison of surface roughness values (predicted and experimental ones) is shown in figure 4 15 This is the same graph as in the figure 4 14 but in terms of Ra values

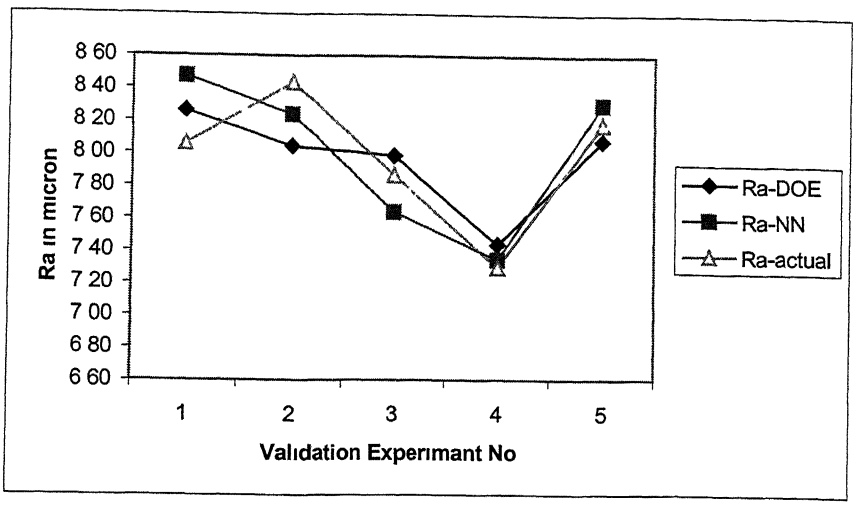


Fig 4 15 Comparison between predicted and experimental values of 'Surface roughness'

Figure 4 16 shows the comparison between predicted (by DOE and NN methods) and experimental values of cutting zone temperature In the first experiment both the predicted values are way different than the experimental one But in the fifth experiment Neural Network fumbles to predict a greater value than the experimental one

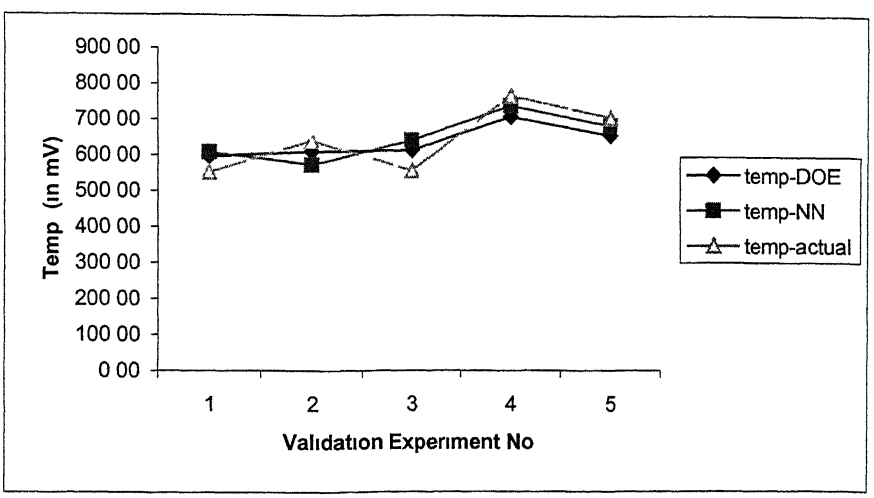


Fig 4 16 Comparison between predicted and experimental values of 'Cutting zone temperature'

### 4.2.2 Comparison between the errors in Design of Experiment and Neural Network predictions

The errors are calculated by using the following formula

$$\% e = 100 * \frac{\text{(Predicted value - Experimental value)}}{\text{Experimental value}}$$

| S\n | Wear %e (DOE) | Wear %e (NN) | s f %e (DOE) | s f %e (NN) | Ra %e (DOE) | Ra %e (NN) | Temp %e (DOE) | Temp %e (NN) |
|---|---|---|---|---|---|---|---|---|
| 1 | 9 06 | 4 41 | -7 14 | -14 50 | 2 50 | 5 13 | 7 89 | 10 04 |
| 2 | 4 90 | 1 98 | 15 74 | 7 99 | -4 65 | -2 34 | -4 72 | -10 49 |
| 3 | 12 28 | 12 45 | -3 94 | 7 48 | 1 50 | -2 89 | 10 05 | 14 98 |
| 4 | 5 18 | 9 27 | -3 81 | -1 33 | 1 92 | 0 66 | -7 57 | -3 64 |
| 5 | 2 92 | 0 22 | 3 96 | -4 40 | -1 26 | 1 47 | -7 14 | -3 35 |

Table 4 5 Errors in prediction by Design of Experiment and Neural Network

Figure 4 17 to Figure 4 20 depict comparisons of the error in predictions for the different response variables by both the prediction techniques i e Design of Experiments and Neural Network

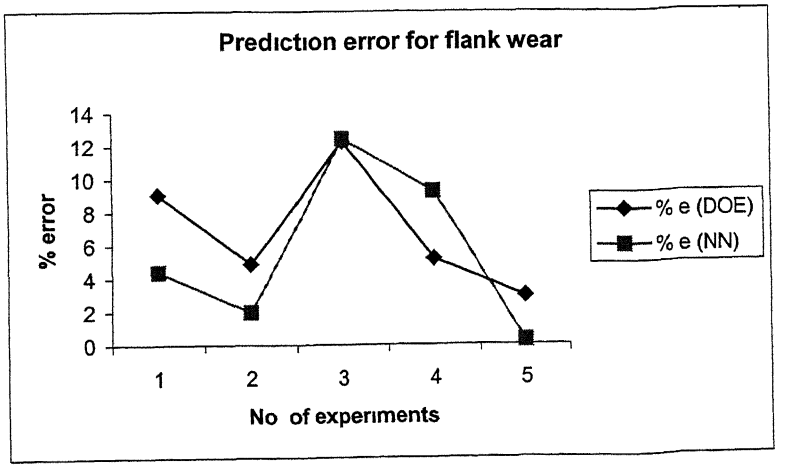


Fig 4 17 Comparison of errors in prediction of 'Flank wear'

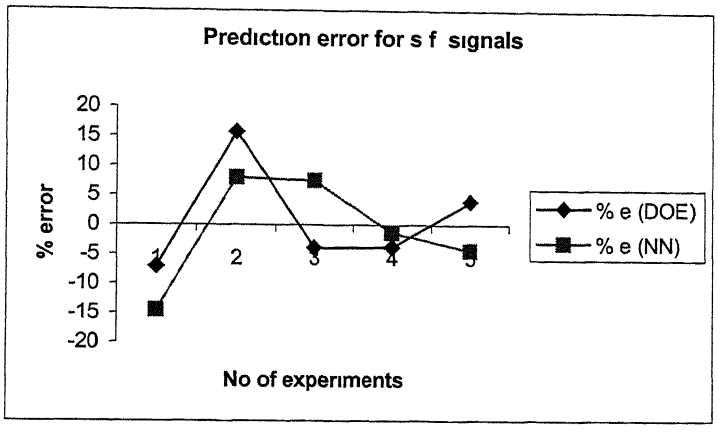


Fig. 4 18 Comparison of errors in prediction of the 'Surface finish signals'

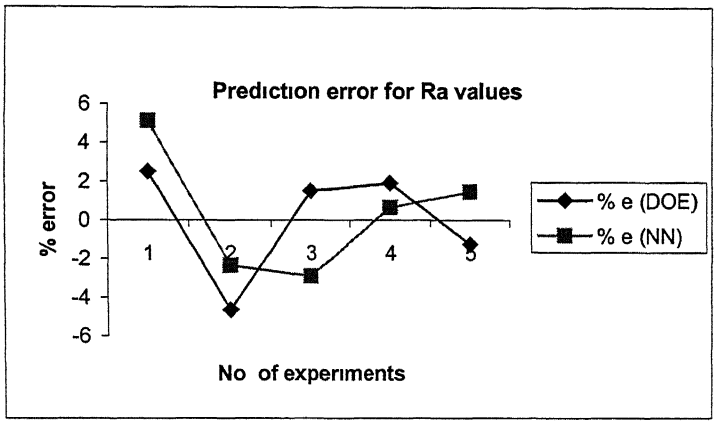


Fig 4 19 Comparison of errors in prediction of the 'Surface roughness'

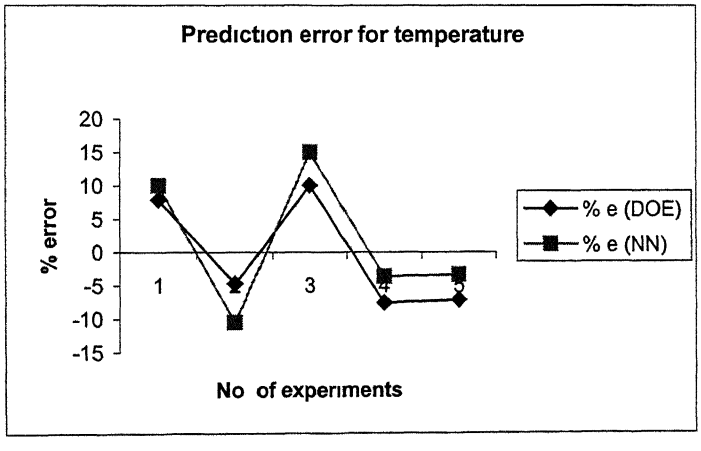


Fig. 4 20 Comparison of errors in prediction of the 'Cutting zone temperature'

| Wear %e (DOE) | Wear %e (NN) | s f %e (DOE) | s f %e (NN) | Ra %e (DOE) | Ra %e (NN) | Temp %e (DOE) | Temp %e (NN) |
|---|---|---|---|---|---|---|---|
| 6 87 | 5 66 | 0 96 | -0 95 | 0 0022 | 0 40 | -0 30 | 1 51 |

Table 4 6 Average errors in the predictions by Design of Experiment and Neural Network

From the table 4 6 it is evident that for our set of data the neural network predicts the flank wear nearer to the experimental values than the Design of Experiment as the average error in prediction is lesser in case of prediction with the Neural Network In the prediction of Surface finish signals, surface roughness values and the cutting zone temperature the average error by both the methods is very small (less than 3 0%) Although there are very large errors in predictions in some of the cases in table 4 5, they can be attributed to some experimental errors

## 4.3 Relationship between Surface roughness and Flank wear

Relationship between the Surface roughness values and the flank wear in the present work, can be represented by the graphs in figures 4 21 (a), (b), (c) These figures show a decrease of flank wear with the increase in Ra values This can be understood from the trends of graph between cutting speed and Ra values and the graph between cutting speed

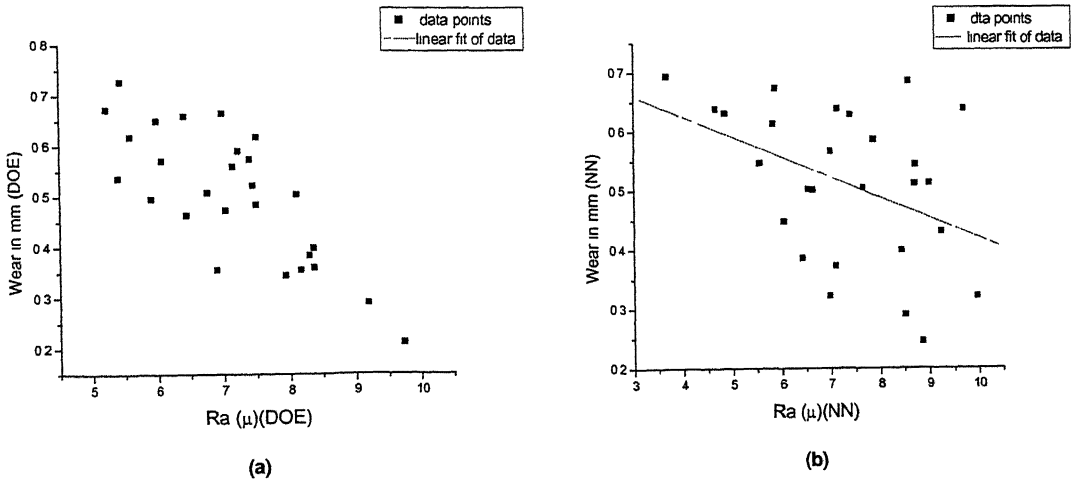


Figure 4 21 Relationship between Ra values and flank wear (a) using DOE predictions (b) using NN predictions

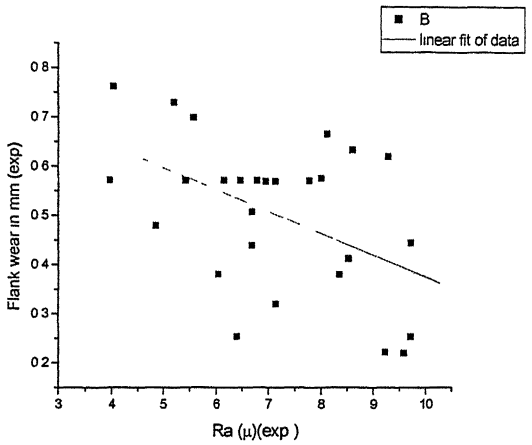


Fig 4 21(c) Relation between Ra values and flank wear using experimental values

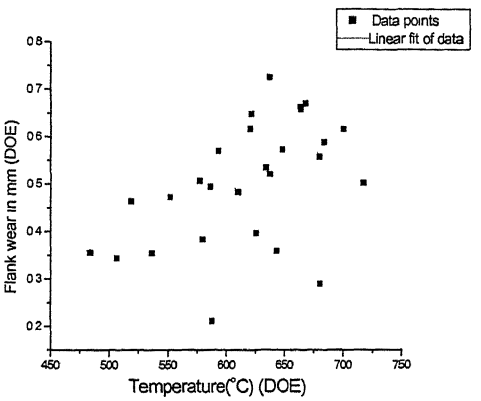


Fig 4 22 (a) Relation between Flank wear and temperature using DOE predictions

and flank wear On high cutting speeds Ra value decreases as the surface finish improves but the flank wear increases and on the low cutting speeds, due to lesser forces the wear is less but also the Ra surface finish deteriorates This may give the reason of the decreasing trend of above graphs

## 4.4 Relationship between Temperature and Flank wear

Figure 4 22 (a) above, and figures 4 22 (b), (c) show the relationship between temperature and the flank wear The trend of the data shows that the temperature increases with the increase in the flank wear Which is in accordance with the theory

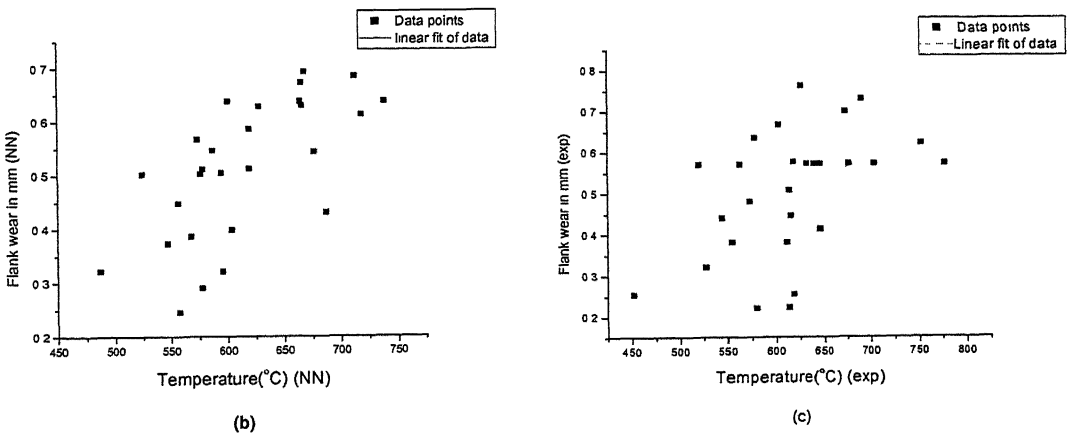


Figure 4 22 Relation between Temperature and Flank wear (b) using NN predictions (c) using experimental values

# Chapter 5

## Conclusion and Scope for future work

## 5.1 Conclusion

An attempt is made in the present work to find out a reliable technique for tool wear prediction After carrying out twenty seven experiments of the training set the regression equations for the response variables (flank wear, surface finish signals, surface roughness values and the temperature) are obtained using the Design of experiment analysis. Neural network is also trained using the experimental values of the response variables for all the twenty-seven experiments of the training set

Predictions of the response variables were made using the Design of Experiments and the Neural Network techniques and the values obtained by both of the methods were compared with the experimental values of the response variables to decide about the nearness of the predictions with the experimental values

In our case, we used low ranges of input variables [Cutting speed (V) = 20 to 35 m/min, feed (F) = 0 075 to 0 125 mm/rev and depth of cut (D) = 0 4 to 0 8] The results showed that Neural Network comes ahead of the Design of Experiment in nearness of the predictions to the experimental values of flank wear as the average errors in the flank wear in case of using Neural Network are less than those obtained using Design of Experiment, while in case of temperature, surface finish signals and surface roughness values both give results with in 2% error so both of them can be termed as reliable

Graphs, showing the relationship between Surface roughness and Flank wear and also between Flank wear and Temperature for both the prediction methods and also for the experimental values, are drawn which shows that the Trends, shown by these graphs for both the prediction techniques and the experimental values, are the same These graphs can help in indirect measurement the flank wear

## 5.2 Scope for future work

The experience gained in using the present system has helped in identifying some of the prospective areas for future as given below

- The neural network program can be interfaced with the machine tool to gather data directly from the machine using Data Acquisition Card
- Surface finish and temperature can be correlated with the vibrations present during machining
- Some other prediction techniques may also be compared
- A more rigid optical fiber system can be used to see the change in results
- White light can be tested for replacing the laser
- Similar comparison work can be done for other machining processes
- Present study can be done by taking some experimental design other than $3^3$ factorial design An increment in the number of level will make the DOE analysis more refined
- Larger number of training data can be used to train the Neural Network program Since the training of the NN program depends upon the number of training samples, more the number of samples, better will be the training

## *References*


[1] G K Lal, 'Introduction to Machining Science', New Age International Ltd Publishers, NewDelhi, INDIA (1996)

[2] G C Sen and A Bhattacharya, 'Principles of Metal Cutting', New Central Book Agency, Calcutta, INDIA (1969)

[3] Li Dan and J. Mathew, 'Tool wear and failure monitoring techniques for turning, a review', Int J. of Machine Tools and Manufacture, Vol.30, No. 4 (1990), pp 579-598

[4] Limin Fu, 'Neural Network in Computer Intelligence', McGraw Hill, Singapore (1994)

[5] Simon Haykin, 'Neural Networks, A Comprehensive Foundation', MacMillian College Publishing Co NewYork (1994)

[6] O Masory, 'Monitoring machining processes using multi-sensor reading fused by Artificial Neural Network', Journal of Materials Processing Technology, 28 (1991) pp 231-240

[7] J H Lee, S J.Lee, 'One step ahead prediction of flank wear using cutting force', Int J. of Machine tools and Manufacture, 39 (1999), pp 1747-1760

[8] Qiang Liu, Yusuf Altintas, 'On-Line monitoring of flank wear in turning with Multi-layered feed forward Neural Network', Int J of Machine Tools and Manufacture, 39 (1999), pp 1945-1959

[9] S K Chaudhury, V K Jain, Ch V V RamaRao, 'On-Line monitoring of tool wear in turning using a Neural Network', Int J of Machine Tools and Manufacture, 39 (1999), pp 489-504

[10] A,Ghasempoor, J Jeswiet, T N Moore, 'Real time implementation of on-line tool condition monitoring in turning', Int J of Machine Tools and Manufacture, 39 (1999), pp 1883-1902

[11] D E Dimla Sr , P M Lister, 'On-line metal cutting tool condition monitoring II . tool state classification using multi-layer perceptron Neural Network', Int J. of Machine Tools and Manufacture, 40 (2000) pp 769-781

[12] David A Dornfeld, 'Neural Network sensor fusion for the tool condition monitoring' , Annals of CIRP Vol39/1/1990, pp 101-105

[13] Choon Seong Leem, D A Dornfeld, S E Dreyfus, 'A customized Neural Network forsensor fusion in on-line monitoring of cutting tool wear', Trans Of ASME, J of Enng Ind , Vol 117, May 1995, pp 152-159

[14] S Purushothaman and Y G Srinivasa, 'A back propogation algorithm applied to tool wear monitoring', Int J of Machine Tools and Manufacture, Vol 34, No 5 ('1994) pp 625- 631

[15] Xiaoli Li, Shen Dong, Zhejun Yuan, 'Discrete wavelet transformation for tool breakage monitoring', Int J of Machine Tools and Manufacture, 39 (1999), pp 1935-1944

[16] D E Dimla Sr , P M Lister, ' On-line metal cutting tool condition monitoring I Force and vibration analysis', Int J of Machine Tools and Manufacture, 40 (2000), pp 739-768

[17] Kunio Uehara, 'Automatic tool wear monitoring in NC turning', Annals of CIRP vol 28/1/1979, pp 39-42

[18] Y Koren (1), A G Ulsoy and K Danai, ' Tool wear and breakage detection using the process model', annels of CIRP Vol 35/1/1986 pp 285-288

[19] J E Kaye, D H Yan, N Popplewell and S Balakrishnan, 'Predicting tool flank wear using spindle speed change', Int J of Machine Tools and Manufacture, Vol 35, No 9 (1995), pp 1309-1320

[20] N Constantinides and S Bennett, 'An investigation of methods for the on-line estimation of tool wear', Int J of Machine Tools and Manufacture, Vol. 27, No 2, (1987), pp 225-237

[21] K Danai, A G Ulsoy, 'A dynamic state model for on-line tool wear estimation in turning', Trans of ASME, J of Engg Ind , Vol 109, Nov 1987, pp 396-399

[22] G H Lim, 'Tool wear monitoring in machine turning', J of Materials Processing Technology, 51 (1995), pp 25-36

[23] S K Chaudhury, S Ramesh, 'On-line tool wear sensing and compensation in turning', J of Materials Processing Technology, 49 (1995), pp 247-254

[24] K C Fan and Y H Chao, 'In-process dimensional control of the work-piece during turning', Precision Engineering, Jan 1991, Vol 13, No 1, pp 27-32

[25] A Sanjanwala, S.K Chaudhury and V K Jain, 'On-line tool wear sensing and compensation during turning operation', Precision Engineering, April 1990,Vol 12, No 2, pp 81-84

[26] P.Cielo, 'Optical techniques for industrial application', Academic Press Inc ,Bostan (1988)

[27] D C. Montgomery, 'Design and Analysis of Experiments', John Wiley and sons, (1984)

[28] 'Tool Engineer's Handbook', American Society of Tool Engineers, N Y McGraw Hill, (1959)

[29] W C Cochran and G M Cox, 'Experimental Design', Asia Publishing House, India (1977)

[30] R S Sirohi and H C Radha Krishna, 'Mechanical Measurements', Wiley Eastern Ltd. India pp 183-186

[31] V M Muttur, 'Thermo-emf analysis of flank wear in turning', M.Tech thesis, Department of Mechanical engineering, IIT Kanpur, India (2001)

# *Appendix*

## Remaining graphs for section 4.1.1

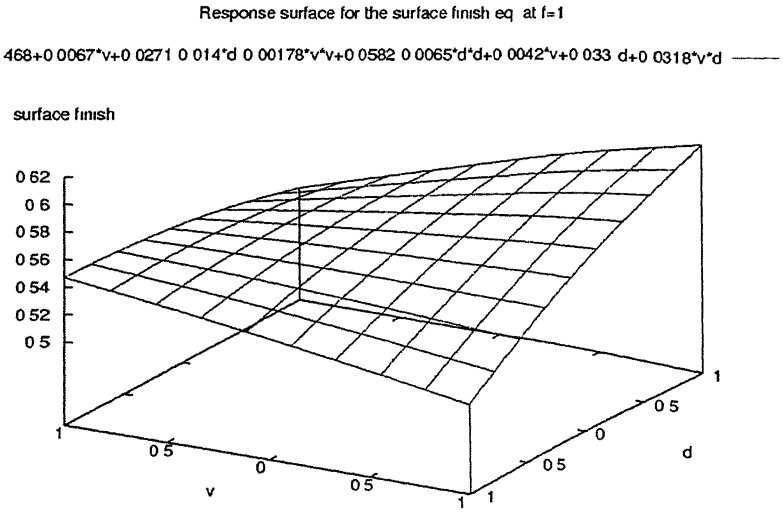


Figure 5 1 Response surface for the regression equation for the Surface finish signals (at f = 1)

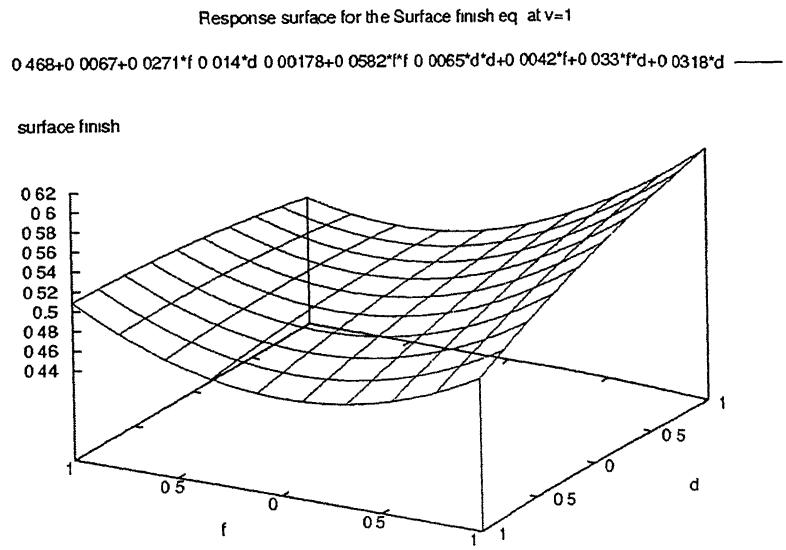


Fig 5 2 Response surface for the regression equation for the Surface finish signals (at v = 1)

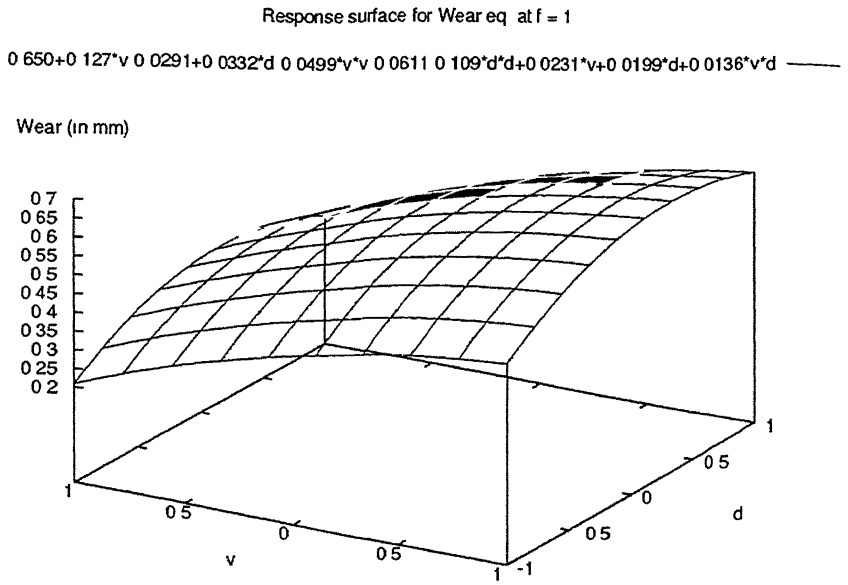


Fig 5 3 Response surface for the regression equation for the flank wear (at f = 1)

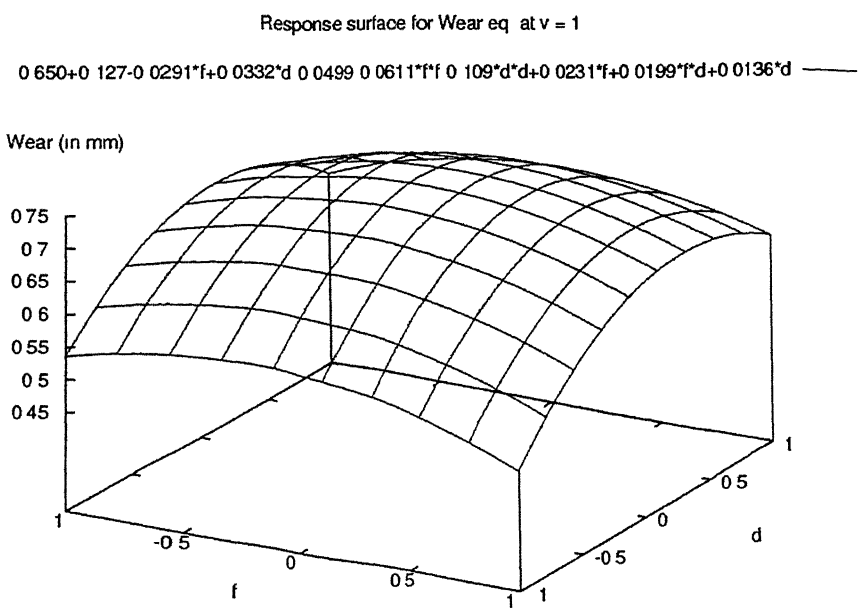


Fig 5 4 Response surface for the regression equation for the flank wear (at v = 1)

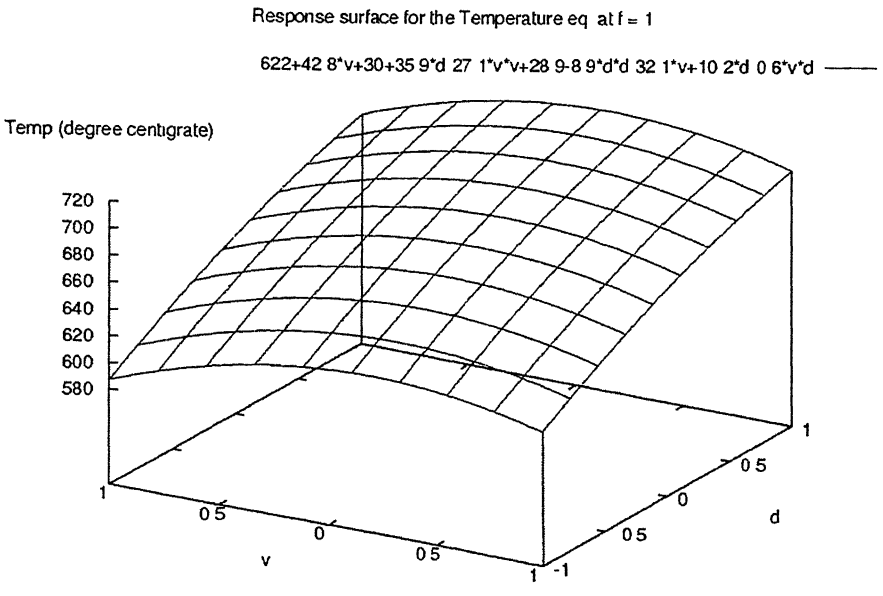


Fig 5 5 Response surface for the regression equation for the temperature (at f = 1)

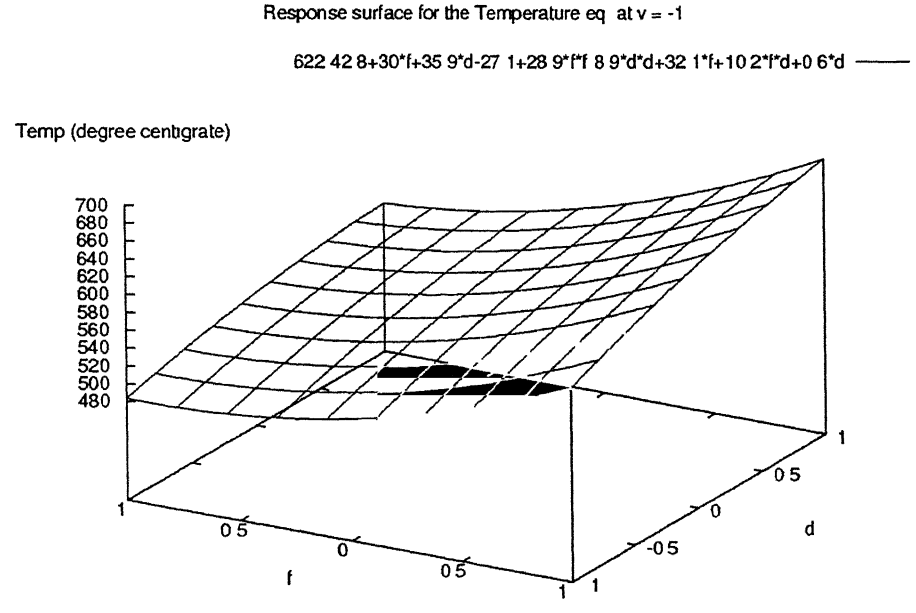


Fig 5 6 Response surface for the regression equation for the Temperature (at v = -1)

## Remaining graphs for section 4.1.2

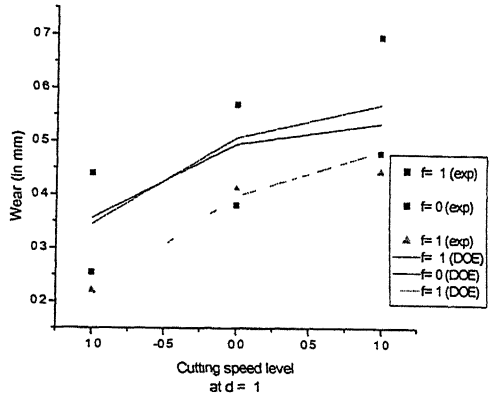


(a)

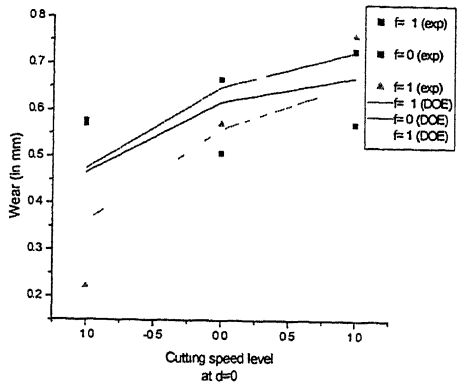


(b)

Fig 5 7 Comparison between DOE predictions and experimental values for Wear (a) at d = -1, (b) at d = 0

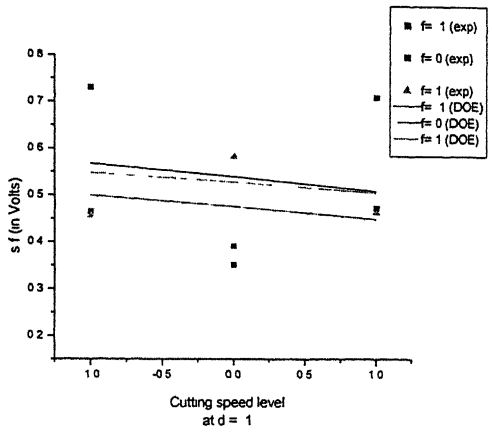


(a)

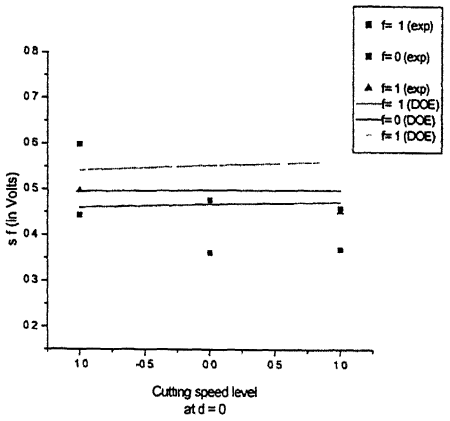


(b)

Fig 5 8 Comparison between DOE predictions and experimental values for Surface finish signals (a) at d = -1, (b) at d = 0

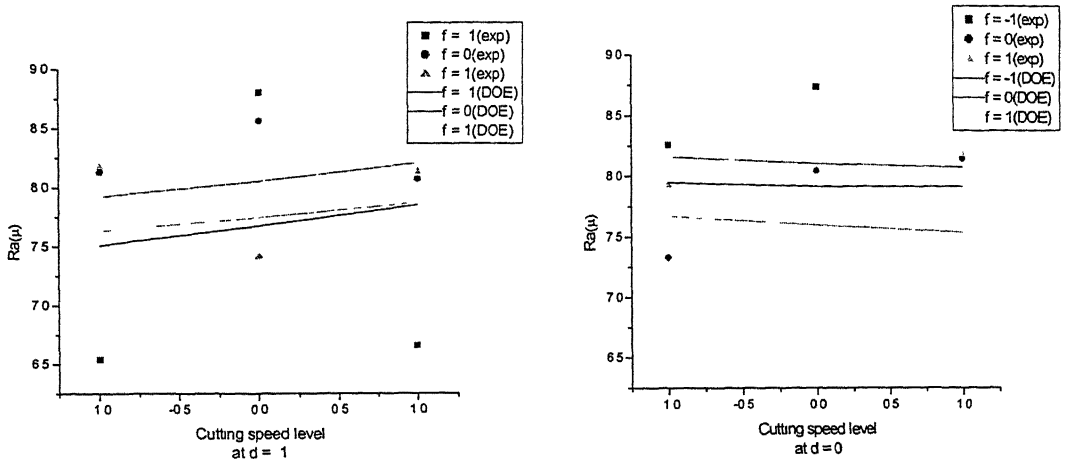


(a) (b)

Fig 5 9 Comparison between DOE predictions and experimental values for Surface roughness (a) at d = -1, (b) at d = 0

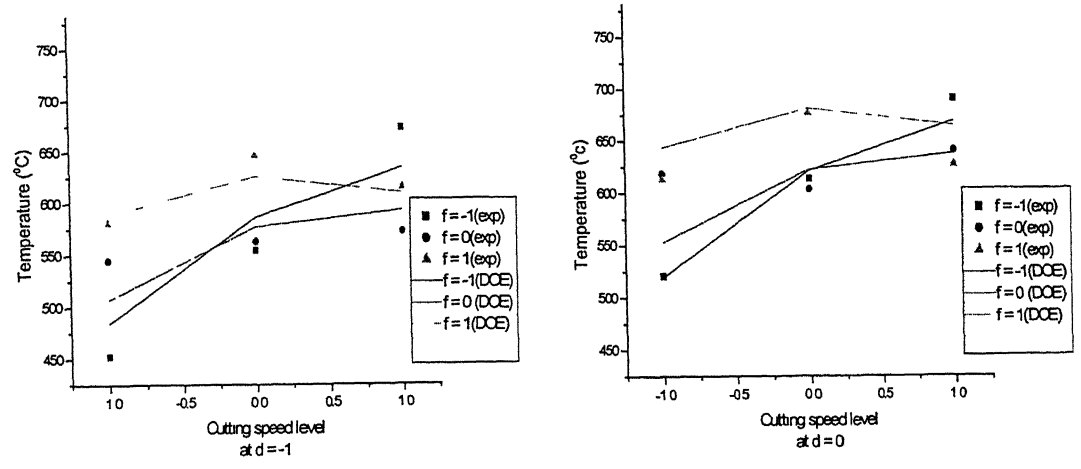


(a) (b)

Fig 5 10 Comparison between DOE predictions and experimental values for Temperature (a) at d = -1, (b) at d = 0

## Remaining graphs for section 4.1.3

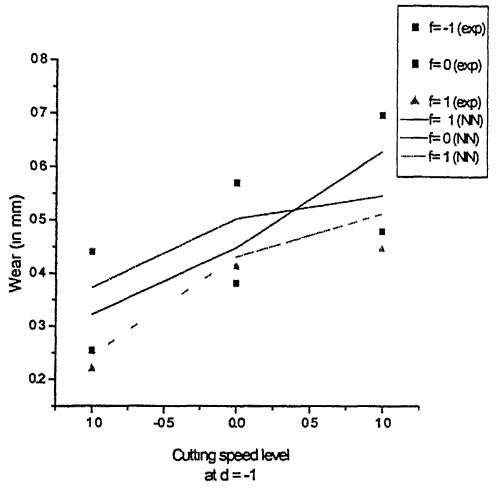


(a)

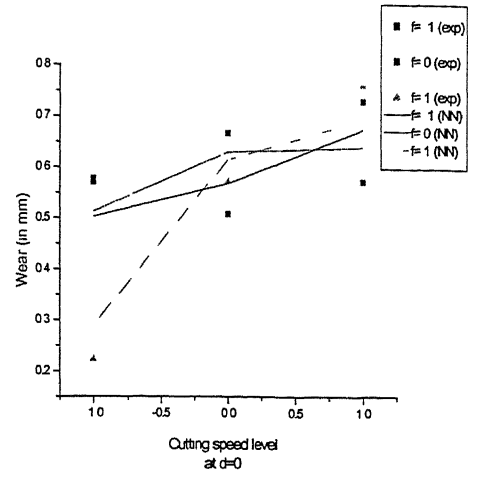


(b)

Fig 5 11 Comparison between NN predictions and experimental values for Wear

(a) at d = -1, (b) at d = 0

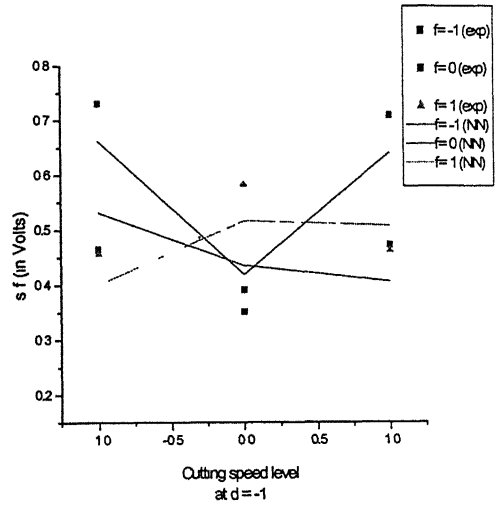


(a)

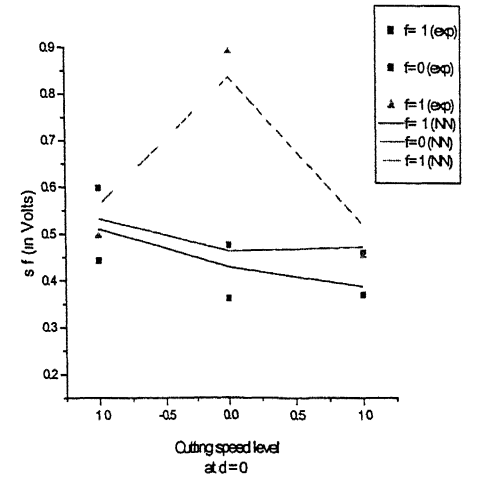


(b)

Fig 5 12 Comparison between NN predictions and experimental values for Surface finish signals

(a) at d = -1, (b) at d = 0

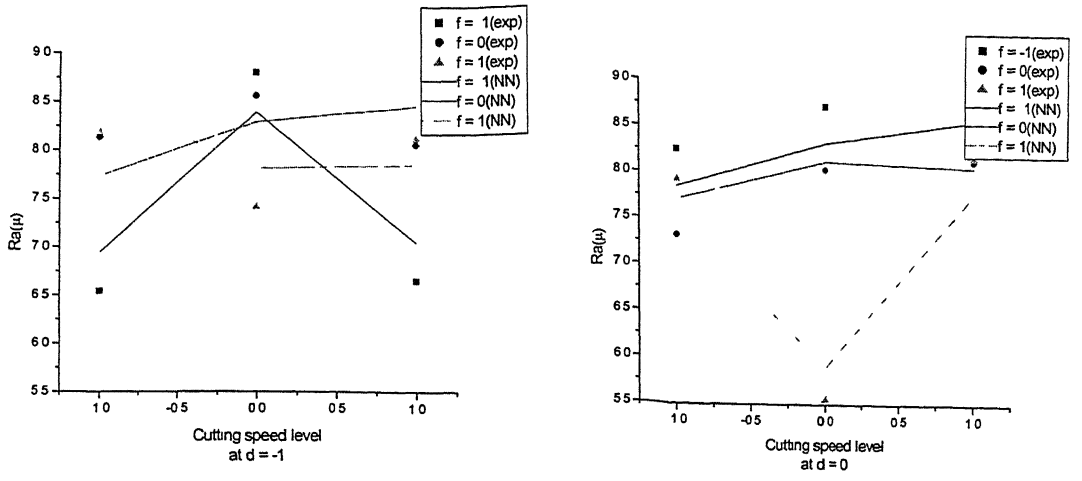


(a) (b)

Fig 5 13 Comparison between NN predictions and experimental values for Surface roughness at (a) d = -1, (b) at d = 0

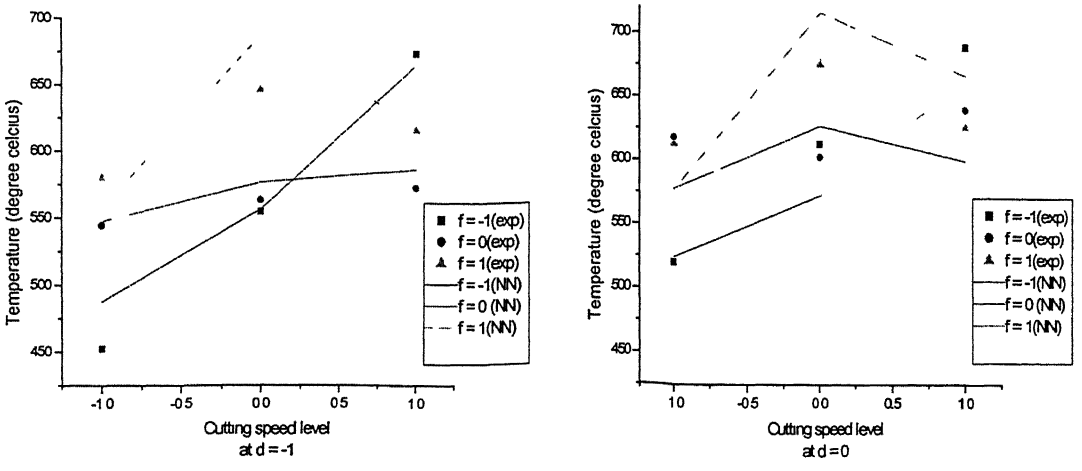


(a) (b)

Fig 5 14 Comparison between NN predictions and experimental values for Temperature at (a) d = -1, (b) at d = 0

- Workpiece material — EN 24 steel
- Workpiece combintion — 0 35 – 0 45 % C, 0 45 – 0 6 % Mn, 1 3 – 1 8 % Ni, 0 9 – 1 4 % Co, 0 2 – 0 3 % Cr, 0 1 – 0 35 % Si, Rest is Iron
- Workpiece hardness — 260 BHN
- Cutting tool material — HSS with 10 % Cobalt
- Cutting tool composition — 18 % W, 4 % Cr, 2 %V, 10 % Co
- Tool geometry — 0°-10°-5°-5°-12°-15°-0 mm
- Specification of lathe — Type LB 25; Center height 250 mm; Center distance: 1500 mm; Swing over bed. 500 mm; Swing over cross slide 330 mm; Spindle speeds 32 – 1600 rpm; Feeds 0 03 – 1.4 mm/rev; 10 HP - 3000rpm motor
- Specifications of Op-amp — Make PMI; Type OP07CP; Power supply total voltage $\Delta V = 30$; Maximum Voltage drift 1 8 $\mu V/\phi C$; Maximum Voltage offset 250 $\mu V$; Maximum current offset 8 nA; Maximum current bias 9 nA; Pin Diagram .on the next page

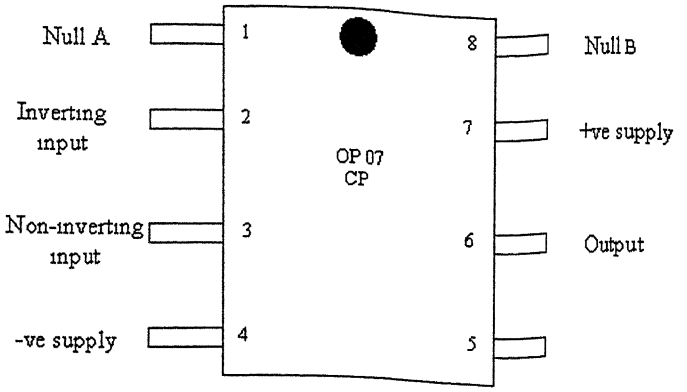
Null A
1
Inverting input
2
Non-inverting input
3
-ve supply
4
OP 07 CP
8
Null B
7
+ve supply
6
Output
5